THE EFFECT OF NET-SPINNING CADDISFLIES ON NITRATE UPTAKE IN STREAM MESOCOSMS

by

Elizabeth Jane Mohr

A thesis submitted in partial fulfillment
of the requirements for the degree

of

Master of Science

in

Land Resources and Environmental Sciences

MONTANA STATE UNIVERSITY
Bozeman, Montana

December 2023

ACKNOWLEDGEMENTS

I wish to thank my advisor Dr. Tim Covino and committee members Dr. Lindsey Albertson and Dr. Rob Payn for all of their support. I also wish to acknowledge the funding sources for my graduate research including the National Science Foundation (Grant DEB-1945941), the United States Department of Agriculture National Institute of Food and Agriculture (Hatch Project 1015745), and the Montana State University Department of Land Resources and Environmental Sciences Ph.D. Fellowship Award.

TABLE OF CONTENTS

TABLE OF CONTENTS CONTINUED

LIST OF TABLES

Table Page

LIST OF FIGURES

Figure Page

LIST OF FIGURES CONTINUED

LIST OF FIGURES CONTINUED

ABSTRACT

Streambeds are thought to play an important role in reducing downstream nitrate export since they provide habitat for microorganisms that use nitrate to build biomass and generate energy. Hydropsychid (net-spinning caddisfly) larvae inhabit the streambed, where they construct silk net and retreat structures. Previous work suggests that the ecosystem engineering activity of net-spinning caddisfly larvae can support higher levels of streambed sediment biomass and create habitat for denitrifying microorganisms, yet it remains unclear whether these effects lead to changes in whole-stream nitrate uptake. We hypothesized that net-spinning caddisflies increase the capacity of the streambed microbial community to take up nitrate. To test this hypothesis, we constructed 15 stream mesocosms and added caddisflies to each according to one of five density treatments ranging from 0 to 2,500 larvae m^{-2}. We measured whole-mesocosm nitrate uptake and characterized hydrologic exchange three weeks after releasing the caddisflies by adding potassium nitrate and sodium chloride to each mesocosm and measuring nitrate + nitrite concentrations over the next 10 hours. To characterize rates of nitrate uptake in the mesocosm streambed, a proxy for the capacity of the streambed microbial community, we used a model that accounts for hydrologic differences among the mesocosms using specific conductance measurements. We found some evidence that higher net-spinning caddisfly densities resulted in higher rates of whole-mesocosm nitrate uptake, or greater nitrate removal. However, we found little evidence that net spinning caddisflies had a substantial effect on nitrate uptake rates in the streambed. We outline several limitations of our study and provide recommendations for improving the experimental set-up and modeling approach in future work. Overall, this research demonstrates some potential for net-spinning caddisflies to serve as ecosystem engineers by altering nitrate removal in streams, though research is needed to lend additional evidence to our findings and to better understand the mechanism by which caddisflies impact nitrate uptake.

INTRODUCTION

Streams and river ecosystems are invaluable natural resources that provide services ranging from supporting fisheries and providing recreational opportunities to supplying drinking water (Opperman et al., 2018). Yet maintaining freshwater ecosystem integrity is challenging when confronted with competing demands. For example, in recent decades humans have drastically altered the global nitrogen (N) cycle through production and application of agricultural fertilizer, contributing to increased crop yields (Guo et al., 2022; Vitousek et al., 1997). However, these activities have also compromised stream and riverine function and associated services by generating excess soluble N that enters streams and rivers from the surrounding landscape and contributes to eutrophication, harmful algal blooms, and hypoxic zones in both receiving and downstream waters (Diaz & Rosenberg, 2008; Hallegraeff, 2003; Smith, 2003; Wurtsbaugh et al., 2019). Resulting economic losses have been conservatively estimated at $2.2 billion dollars annually in the United States alone (Dodds et al., 2009). Moreover, financial investments in measures aimed at alleviating N pollution have been largely unsuccessful in part due to legacy N in soil and groundwaters, highlighting the long-term nature of this problem (Basu et al., 2022).

The potential for eutrophication and its effects can be mitigated by the capacity of stream and river ecosystems to take up and transform inorganic N before it reaches downstream waters (Breemen et al., 2002; Schlesinger et al., 2006). Nitrate (NO_3^-) is the dominant form of inorganic N in streams and rivers (Helton et al., 2015), and it can be removed from the stream water column via denitrification, annamox, and assimilation (Burgin & Hamilton, 2007; Zhang et al., 2020). Denitrification refers to a microbial process where NO_3^- is reduced to N_2, usually coupled

with organic carbon oxidation. Similarly, annamox (anaerobic ammonia oxidation) is a microbial process where ammonia is oxidized and NO_3^- is reduced, yielding N_2. Because denitrification and annamox both yield N_2, they are considered "permanent" N removal pathways. Moreover, both processes occur most commonly under low oxygen conditions (Burgin & Hamilton, 2007; Zhang et al., 2020), including in "microzones" of anoxia that can form in bulk-oxic pore waters (Briggs et al., 2015). Assimilation refers to a process where organisms, including microbes and plants, incorporate N from NO_3^- into their biomass (Burgin & Hamilton, 2007; Zhang et al., 2020). Following assimilation, N in biomass can be mineralized and return to the stream water as soluble inorganic N, move up the food chain and be exported to the terrestrial sphere, or can be subsequently denitrified (Hall et al., 1998; Hauer et al., 2016; Seitzinger et al., 2006; Zhang et al., 2020). The total change in stream water NO_3^- concentration resulting from denitrification, annamox, assimilation, and remineralization is referred to here as "overall net nitrate uptake."

Streambeds play an important role in nitrate uptake since they provide habitat for microorganisms that assimilate and denitrify NO_3^- (Battin, Kaplan, Newbold, & Hansen, 2003). The process of hyporheic exchange – the bidirectional exchange of water between the stream channel and stream bed – facilitates nitrate uptake in the streambed by delivering electron donors, acceptors, and nutrients to the streambed microbial community (Boulton et al., 2010; Covino, 2017; Hinkle et al., 2001; Li et al., 2021). The rate of hyporheic exchange (i.e., the fraction of the stream channel that exchanges with the streambed, per unit time) can thus regulate net nitrate uptake rates by controlling the rate at which nitrate is delivered to the biologically active streambed. Further, the likelihood that nitrate molecules are taken up in the streambed before returning to the channel is governed by both the metabolic activity of the streambed,

characterized by the "streambed nitrate uptake rate" in this study, and the amount of time that water introduced to the hyporheic zone spends in the streambed before returning to the channel, referred to here as "streambed travel time" (Gomez-Velez et al., 2015; Li et al., 2021; Zarnetske et al., 2012). When streambed nitrate uptake occurs rapidly compared to streambed travel time, nitrate uptake is considered "exchange limited" because only an increase in hyporheic exchange rate would lead to appreciably greater rates of overall net nitrate uptake rate. Conversely, nitrate uptake is considered "reaction limited" when streambed nitrate uptake occurs slowly relative to the average streambed travel time (Harvey et al., 2013; Zarnetske et al., 2012).

In addition to the characteristics of hyporheic exchange, many other factors are thought to influence nitrate uptake rates in streams, including availability of dissolved organic carbon and oxygen, gross primary production, and microbial community composition (Gonzalez-Pinzon et al., 2021; Hall et al., 2009; Zarnetske et al., 2012). Another potentially overlooked factor is the activity of ecosystem engineers, or organisms that impact ecosystem function by altering their physical environment (Hastings et al., 2007; Jones et al., 1994). Net-spinning caddisfly (Trichoptera: *Hydropsychidae*) larvae are ecosystem engineers that inhabit streambed sediment, where they build net and retreat structures out of silk (Morse et al., 2019). These structures can bind together sediment grains, increasing streambed stability and reducing flow velocities in the interstitial spaces of the streambed (Cardinale et al., 2004; Hemphill, 1988; Juras et al., 2018). In a recent study, MacDonald et al. reported higher amounts of ash-free dry mass in the presence of hydropsychid larvae compared to in their absence (MacDonald et al., 2020), suggesting that net-spinning caddisfly larvae support greater levels of microbial biomass. Further, Bertagnolli et al. recently showed that relative to adjacent rock biofilm, caddisfly silk structures were enriched in

microbial taxa with known roles in nitrification and denitrification and were enriched in specific genes implicated in denitrification (Bertagnolli et al., 2023). Together these findings suggest that caddisfly silk structures have the potential to alter streambed nitrogen cycling and therefore whole-stream nitrate uptake, though this has been rarely tested experimentally (Tumolo et al., 2023).

In this study, we tested the hypothesis that net-spinning caddisflies influence overall net nitrate uptake by increasing the capacity of the streambed microbial community to transform nitrate. To do this, we constructed 15 stream-analogue mesocosms and manipulated caddisfly larval density using five experimental treatments ranging from 0 to 2500 caddisflies m^{-2}. Sixteen days after adding the caddisfly larvae, we characterized rates of nitrate uptake and hyporheic exchange in each mesocosm by releasing reactive nitrate and conservative sodium chloride tracers. We fit a linear regression to the nitrate time-series to estimate overall net nitrate uptake rate in each mesocosm. To characterize the capacity of streambed microbes to take up nitrate in each mesocosm, we estimated streambed nitrate uptake rates by fitting a process-based model that accounted for variation in hydrologic characteristics among the mesocosms. Finally, we used continuous dissolved oxygen measurements to estimate gross primary production (GPP) and aerobic ecosystem respiration (AER) in each mesocosm to characterize additional potential influences on nitrate uptake. Overall, the mesocosm experiments and modeling allowed us to examine the effect of caddisfly density on overall net nitrate uptake and streambed nitrate uptake while considering other factors including hyporheic exchange, GPP, and AER.

METHODS

Mesocosm Experiment

Mesocosm Design

Each of the 15 mesocosms consisted of two cylindrical polyethylene tanks nested to form a circular stream channel analog with a 9-cm width and a 56-cm outer diameter (Figure 1). The channels were filled with gravel (diameter median = 19 mm, interquartile range = 11 mm) that had been incubated in mesh laundry bags submersed in Cherry Creek, Montana (45.613, -111.517) from January 8, 2021 to August 4, 2021. We shaped the incubated gravel (hereafter gravel) into a single dune (maximum height = 20 cm, minimum height = 10 cm) to facilitate the exchange of water between the streambed and stream channel. After shaping the gravel, we collected rocks (diameter median = 4.4 cm, interquartile range = 2.1 cm) from the surface of the riverbed in Cherry Creek (45.600, -111.496) and removed any visible macroinvertebrates. We then covered the subsurface dune with a single layer of surface rocks to ensure that each mesocosm contained an active community of photosynthetic microorganisms.

Each mesocosm also contained enough artificial stream water to bring the water surface to 30 cm from the base of the mesocosm, which was maintained by a drain tube. Artificial stream water consisted of dechlorinated tap water, fulvic acid, 0.14 ppb NO_3^--N and a variety of micronutrients (Table 1), a formulation that was modified from (Bastviken et al., 2004). We used submersible pumps (VIVOSUN 210 GPH Submersible Pumps) placed at the top of each dune to circulate water around the channel of each mesocosm.

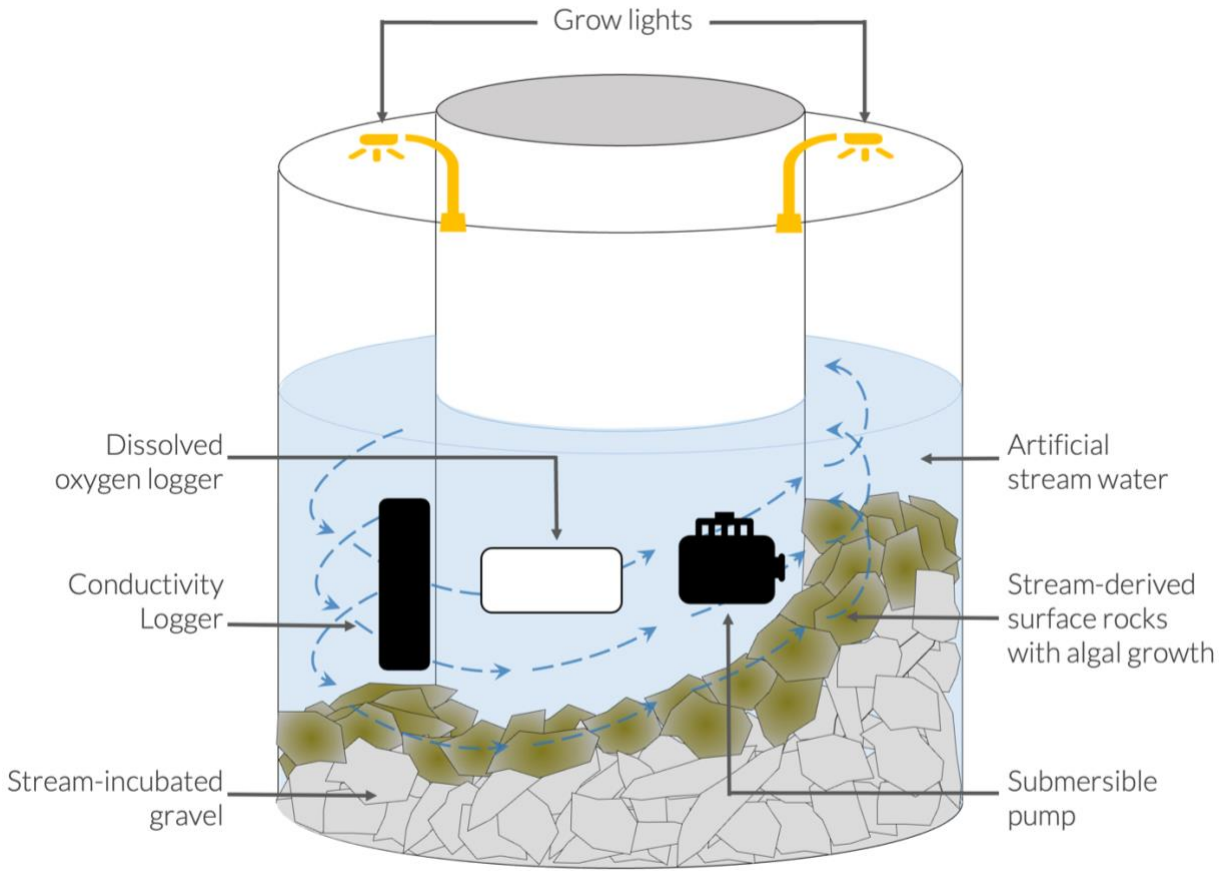

Figure 1. Diagram showing key components of the mesocosm setup including two nested cylindrical tanks, stream-incubated rocks, algae, artificial stream water, a pump, a dissolved oxygen logger, a conductivity logger, and two LED grow lights.

To stimulate primary production in the mesocosms, we equipped each with two LED grow lights (Relassy LED Full Spectrum Grow Lights for Indoor Plants) placed midway between the dune peak and trough on either side of the dune. The lights were programmed to turn on at ~6:45 am and off 12 hours later to simulate natural diel variations in light availability. We kept overhead lights off for the duration of the experiment and covered all windows with a UV-blocking film. We also controlled water temperature using a chiller and pump to circulate cold water through shrink-wrapped, copper tubing that hugged the interior wall of each mesocosm. This set-up kept the water temperature in each mesocosm consistently between 15.5 and 17 °C.

Finally, each mesocosm was outfitted with a PME MiniDOT® Logger programmed to measure and record dissolved oxygen concentrations and water temperature at 10-minute intervals, and an Onset HOBO U24-001 Fresh Water Conductivity Data Logger programmed to measure electrical conductivity and temperature of the water at 10-minute intervals.

Table 1. Artificial stream water composition

Chemical	**Concentration (mg L^{-1})**
$CaCl_2$	8
$CoCl_2$	0.02
$CuSO_4$ x 5 H_2O	0.02
$FeCl_3$ x $6H_2O$	1.4
$KHCO_3$	10
$MgSO_4$ x $7H_2O$	4
MnCl2 x $4H_2O$	0.36
$NaHCO_3$	10
Na_2MoO_4 x $2H_2O$	0.0042
$ZnSO_4$ x $7H_2O$	0.044
Fulvic Acid	2.3
KNO_3*	0.001

*KNO_3 was added starting on August 21, 2021

Mesocosm Acclimation

After creating the simulated streambeds from August 4th to August 6th, 2021, we allowed them to acclimate for 26 days. During this acclimation time, we allowed consistent flow into and out of each mesocosm at a rate of roughly 35 liters per day. The water flowing into each mesocosm consisted of 20% fresh artificial stream water (Table 1) with the remaining 80% of mixture consisting of recycled water that had recently flowed out of all 15 mesocosms into a central mixing reservoir. While the former ensured that each mesocosm received a steady supply of carbon and nutrients during the acclimation period, we intended the latter to promote exchange of microbial communities among mesocosms.

Caddisfly treatments

Following the acclimation period, we randomly assigned each mesocosm to one of five caddisfly larvae density treatments: 0, 100, 300, 850, or 2,500 caddisflies m^{-2}, equivalent to 0, 16, 47, 133, or 390 caddisflies added. We then released the appropriate number of caddisflies into each mesocosm on September 1st, 2021 and allowed the caddisflies to build their silk structures for 16 days before performing tracer tests to measure nitrate uptake. During this colonization period, the mesocosms were maintained as during the acclimation period. To provide the caddisflies with a food source, we added 200 mg of algae wafers (Hikari® Tropical Algae Wafers™), finely powdered with a mortar and pestle, to each mesocosm on September 2nd, September 4th, September 7th, and September 10th.

Hydrologic Exchange and Nitrate Uptake Characterization

Sixteen days following the caddisfly addition, we characterized hyporheic exchange and nitrate uptake in each mesocosm by disconnecting the mesocosms from the flow-through system and adding 10 mL of slug solution containing 2.31 M NaCl and 0.04 M KNO_3 (547 ppm NO_3-N). The instantaneous tracer addition rapidly raised specific electrical conductivities by about 125 μS cm^{-1} above background levels and raised NO_x (NO_2^- + NO_3^-) concentrations by about 220 μg L^{-1} NO_x-N above background concentrations, which were less than 8 μg L^{-1} NO_x-N in all mesocosms.

To characterize hyporheic exchange, we measured and recorded conductivity and temperature at 1 second intervals for at least 30 minutes following the slug solution addition using Onset HOBO U24-001 Fresh Water Conductivity Data Loggers ("HOBO loggers"). We standardized conductivity readings across HOBO loggers by measuring electrical conductivity

and temperature in each mesocosm on 18 days between August 20th and September 20th using a portable conductivity meter (Thermo Scientific™ Orion Star™ A329 Portable Multiparameter Meter, hereafter referred to as the "Orion meter"). For each HOBO logger, we built linear regressions for both conductivity and temperature describing the relationship between HOBO logger readings and Orion meter readings. We then used these regressions to estimate a meter-standardized conductivity (σ) and temperature (T) value for each logger reading. Finally, we calculated specific conductance (SC, σ_{SC}) using the linear relationship:

$$\sigma_{SC} = \frac{\sigma}{1 + 0.02(T - 25)}$$

To estimate added salt concentration from background-corrected SC, we developed a linear relationship between the concentration of added salt and background-corrected SC. First, we incrementally added 7, 83-µL volumes of a 2.3 M NaCl, 0.045 M KNO_3 solution to a 1-liter volume of artificial stream water and measured the resulting SC after each addition using the Orion meter. Next, we calculated background-corrected SC by subtracting the SC measured in the artificial stream water solution before any salt solution was added. We then fit a simple linear regression to these data to characterize the relationship between added NaCl concentration and background-corrected SC. To calculate background-corrected SC for each mesocosm, we first calculated background SC as the average SC measured during the 30 minutes prior to the slug addition and then subtracted this value from all SC measurements following the slug addition. Finally, we used the slope from the linear relationship described above to estimate added salt concentration from background-corrected SC.

To characterize nitrate uptake, we measured nitrate + nitrite (NO_x) concentrations over time by collecting water samples prior to the tracer addition and roughly 10 min, 40 min, 1.5 hr,

2.5 hr, 3.5 hr, 4.5 hr, 6 hr, 8 hr, 10 hr, and 24 hr following the KNO_3 addition. We collected all samples using acid-washed syringes that had been triple rinsed with sample. We filtered the samples using 0.2-μm PES syringe filters (Cytiva Whatman Uniflo), first using the filtered sample to triple-rinse acid-washed, high-density polyethylene bottles before filling them with 30 mL of filtered sample. Samples were stored in the freezer prior to analysis for NO_x concentrations by colorimetry at the Flathead Lake Biological Station's Freshwater research lab. While we report these concentrations as "NO_x" in the results, the NO_x in our samples was likely composed primarily of nitrate since we added potassium nitrate to the mesocosms and since nitrite typically does not accumulate in well-lit systems (Zhang et al., 2020). Therefore, for simplicity we refer to the net removal of NO_x characterized by the tracer data as "nitrate uptake" rather than "NO_x uptake".

Post-release Caddisfly Sampling

Following characterization of hydrologic exchange and nitrate uptake, we deconstructed the mesocosms and counted the number of caddisflies recovered from each mesocosm. We observed substantial and consistent caddisfly mortality across treatments (Figure 2). Caddisfly mortality rates – the number of caddisflies that were not recovered at the end of the experiment compared to the number of caddisflies added – ranged from 25% to 71%, with a mean of 52%. While it is not clear whether the caddisflies died before or after influencing the streambed with their net-spinning activities, we believe that caddisflies that died likely did so early in the experiments and that the final caddisfly counts are more representative of caddisfly activity within each mesocosm. Therefore, we report results from analyses that used final caddisfly counts as a predictor rather than caddisfly treatment. However, we note here that analyses yield

similar results when caddisfly treatment is used as the predictor, and we provide these results in Appendix C.

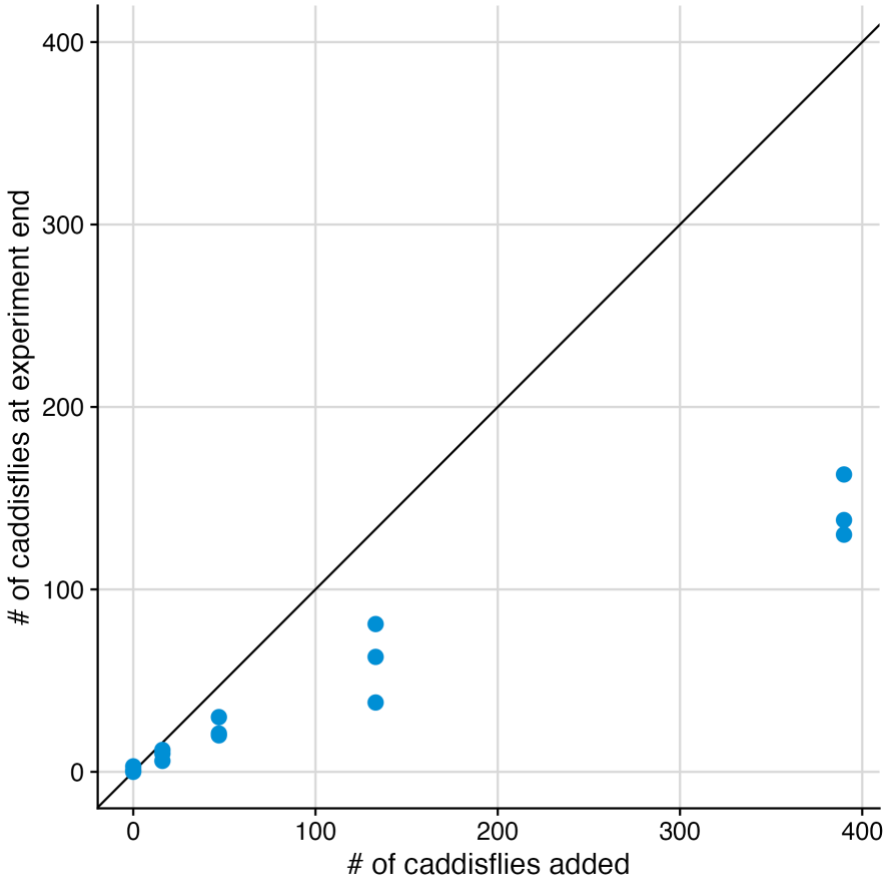

Figure 2. Number of caddisflies counted at the end of the experiment plotted against the number of caddisflies added, with a black 1:1 line showing the no-mortality case.

Modeling the Experimental Data

Overall Net Nitrate Uptake Rate Estimation

We quantified the overall net nitrate uptake rate in each mesocosm by estimating the slope of NO_x concentration as a function of time elapsed following the slug addition. This model assumes that NO_x is transformed according to zero-order kinetics. We used the brms package (Bürkner, 2017) in the R programming language to fit a linear regression to data from each

mesocosm. Because the relationship between NO_x concentration and elapsed time was only linear for NO_x concentrations greater than 50 ppb NO_x-N, we excluded measurements that fell below the 50 ppb NO_x-N threshold. Slope estimates therefore represent a maximum or "saturated" rate of overall net nitrate uptake.

Hyporheic Exchange Rate Estimation

We characterized hyporheic exchange in each mesocosm to control for differences among mesocosms when estimating streambed nitrate uptake rates. To estimate hyporheic exchange rates, we fit a solution of the following model of the change in conservative solute concentration (C) over time to each mesocosm's added-NaCl concentration time-series:

$$\frac{dC}{dt} = q\left(\int_0^t g(\tau)C(t - \tau)\,d\tau - C(t)\right) + C_0\delta(t - t_{add}) \quad (1)$$

In this equation, t represents time, where $t = t_{add} = 0$ at the moment when the slug solution was added, q is the rate of hyporheic exchange expressed as the fraction of channel volume exchanging with the streambed per unit time, τ represents hyporheic travel time defined as the amount of time water spends in the streambed before returning to the channel, and $g(\tau)$ is a probability density function describing the distribution of hyporheic travel times. C_0 is the concentration of added solute in the channel immediately after addition ($t = 0$), and $\delta(t)$ is a Dirac Delta function which is infinite at $t = t_{add}$, and 0 otherwise.

To describe the distribution of streambed travel times in the mesocosms, or $g(\tau)$, we used an exponential model:

$$g(\tau) = \lambda e^{-\lambda\tau} \quad (2)$$

where λ is an unknown shape parameter. With this assumption, Equation (1) can be solved analytically using Laplace transforms (Appendix A) to yield the following solution:

$$C(t) = C_0 e^{-0.5*(\lambda+q)*t} * (\cosh(0.5(\lambda+q)t) + \frac{\lambda - q}{\lambda + q} \sinh(0.5(\lambda+q)t) \quad (3)$$

At steady state (i.e., when the rate of water entering the streambed is equal to the rate of water returning to the channel), the relationship between mean travel time in the streambed ($\bar{\tau}$), streambed pore water volume (V_{sb}), and hyporheic exchange rate (Q) is given by the fundamental relationship $Q = \frac{V_{sb}}{\bar{\tau}}$. For the exponential travel time distribution given in Equation 2, $\bar{\tau}$ is given by $\frac{1}{\lambda}$, and the rate of hyporheic exchange can be calculated as q multiplied by stream channel water volume (V_{ch}). Thus, given values of λ,V_{sb}, and V_{ch}, q can be calculated using Equation 4:

$$q = \lambda * \frac{V_{sb}}{V_{ch}} \quad (4)$$

Further, the following mass conservation relationship holds:

$$V = \frac{V_{add} C_{add}}{C_f} = V_{ch} + V_{sb} \quad (5)$$

where V is total mesocosm water volume, V_{add} is the volume of slug solution added to each mesocosm, C_{add} is the concentration of salt in the slug solution, and C_f is the concentration of added salt in the mesocosm water after the water in the channel and streambed had fully mixed following the salt solution addition. We calculated C_f as the average added salt concentration

during the period spanning 30 minutes to 60 minutes following the slug addition. We then estimated total water volumes (V) for each mesocosm using known values for V_{add} and C_{add}.

We assumed that the slug solution mixed rapidly in the mesocosm channel water upon addition such that the initial condition can be calculated as follows:

$$C_0 = \frac{C_h(V_{ch} - V_{add}) + C_{add}V_{add}}{V_{ch}} \quad (6)$$

where C_h is the concentration of solute prior to the slug addition. Because we corrected concentrations for background, C represents the concentration of added solute and C_h is assumed to be zero. Together, equations (4), (5), and (6) allowed us to estimate the three unknowns needed to solve equation (3) (λ, q, and C_0) by treating λ and V_{sb}/V_{ch} as the parameters to be estimated with Bayesian inference.

Streambed Nitrate Uptake Rate Estimation

To estimate the rate of streambed nitrate uptake (k_{sb}) in each mesocosm, we fit the NO_x concentration data to a model similar to equation (1) that also accounts for reactive solute uptake:

$$\frac{dC}{dt} = q\left(\int_0^t g(\tau)(C(t - \tau) - k_{sb}\tau)d\tau - C(t)\right) + C_{add}\delta(t - t_{add}) \quad (7)$$

Equation (7) assumes that nitrate uptake in the streambed occurs at constant rate (i.e., follows zero-order kinetics). Because this assumption is only reasonable for concentrations of greater than 50 μg L^{-1} NO_x-N, we fit the model only to data satisfying this criterion to obtain a measure of apparent maximum streambed biological activity for each mesocosm. We treated k_{sb} as an

unknown to be estimated by fitting Equation 7 to background-corrected NO_x data. We also estimated the initial concentration of background-corrected NO_x in the mesocosm channel immediately after the tracer release ($C_{0,\,NOx}$). Because Equation (7) is not as analytically tractable as Equation (1), we solved it numerically using the DifferentialEquations.jl package in the Julia programming language (Rackauckas & Nie, 2016).

Parameter Inference for SC and Nitrate Models

To estimate unknown parameters (λ, V_{sb}/V_{ch}, k_{sb}, and $C_{0,\,NOx}$) while quantifying parameter estimate uncertainty, we used a Bayesian modeling approach. Since λ and V_{sb}/V_{ch} are shared parameters among the conservative and reactive tracer models, we fit the models to both the background-corrected NaCl and NO_x datasets simultaneously. For any set of parameters, Equations (1) and (7) can be solved to generate predicted concentrations of added NaCl and NO_x ($C_{pred,\,i}$). To model the data ($C_{obs,\,i}$), we assumed normally distributed error around the model prediction, i.e., $C_{obs,\,i} \sim \text{Normal}(C_{pred,\,i}, \sigma_{obs,i})$ where the standard deviations of the error distributions for both NaCl and NO_x concentrations ($\sigma_{obs,i}$) were additional parameters to be estimated. Given limited prior knowledge about the hydraulic and biogeochemical behavior of our mesocosm setup, we used prior distributions that were minimally informative but within the realm of reason:

$$\lambda \sim Uniform(lower\ bound = 0.0001, upper\ bound = 0.1)$$

$$\frac{V_{sb}}{V_{ch}} \sim Uniform(lower\ bound = 0.1, upper\ bound = 0.9)$$

$$k_{sb} \sim Uniform(lower\ bound = 1e-6, upper\ bound = 1.0)$$

$$\sigma_{obs,NaCl} \sim Half-Cauchy(\mu = 0, \sigma = 5, lower\ bound = 0, upper\ bound = \infty)$$

$$\sigma_{obs,NOx} \sim Half - Cauchy(\mu = 0, \sigma = 25, lower\ bound = 0, upper\ bound = \infty)$$

We sampled posterior distributions using the No U-turn Sampler (NUTS) from the Turing package in the Julia programming language (Ge et al., 2018). We used a target acceptance rate of 0.65 and ran four Markov Chain Monte Carlo (MCMC) chains which generated 1,000 adaptation samples and 2,000 saved samples.

Metabolism Modeling

We used the dissolved oxygen (DO) time-series data from each mesocosm to estimate daily gross primary production (GPP, mg O_2 L^{-1} day^{-1}), aerobic ecosystem respiration (AER, mg O_2 L^{-1} day^{-1}), and normalized gas exchange (k_{600}, day^{-1}) on all 13 days that did not have salt slug additions between September 2nd, 2021 to September 21st, 2021. To estimate metabolism parameters, we fit the DO data to the following model:

$$\frac{dO_2}{dt} = PAR * GPP - ER + (k_g + \frac{Q_{flow-through}}{V})(O_{2,sat}(t) - O_2(t)) \quad (8)$$

where O_2 is dissolved oxygen concentration, $Q_{flow\text{-}through}$ is the rate of water entering the mesocosms from the mixing reservoir described above, and $O_{2,\,sat}$ is the concentration of dissolved oxygen at saturation. The instantaneous gas exchange rate coefficient (k_g) can be normalized to a Schmidt number of 600 using the following relationship (Jähne et al., 1987)

$$k_g = k_{600}\left(\frac{s_A + s_B T + s_C T^2 + s_D T^3}{600}\right)^{s_E} \quad (9)$$

where T is temperature in degrees C, and s_A, s_B, s_C, s_D are Schmidt number coefficients and s_E is a scaling exponent. To calculate k_g, we used temperature data from the MiniDOT loggers along

with the "convert_k600_to_kGAS" function in the streamMetabolizer package (Appling, Hall, et al., 2018), which implements Equation 9 using published values of s_A, s_B, s_C, s_D, and s_E (Raymond et al., 2012). Calculating k_g allowed us to estimate a single gas-exchange parameter (k_{600}) for each day and mesocosm while accounting for variations in water temperature throughout the day. We calculated $O_{2,\,sat}$ using temperature measurements recorded by the MiniDOT loggers and barometric pressure measurements recorded by a HOBO U20 Water Level Logger along with the relationship in (Garcia & Gordon, 1992) implemented as the "garcia-benson" model in the streamMetabolizer R package (Appling, Read, et al., 2018). We calculated water volumes (V) by first using Equation 5 to estimate each mesocosm's total water volume on five dates with NaCl releases (September 3rd, 8th, 11th, 14th, and 20th) and then calculating the average volume across dates for each mesocosm.

We fit equation (8) to the DO data using a Bayesian approach implemented in the probabilistic programming language "Stan" (Carpenter et al., 2017). We used the trapezoidal rule to numerically integrate equation (8) and modeled observation error as independent and identically distributed ($O_{2,\,obs} \sim \text{Normal}(O_{2,\,pred}, \sigma_{obs})$). Our model included prior probability distributions synthesized in previous research (Appling, Hall, et al., 2018; Hall et al., 2016; Raymond et al., 2012) and divided by target surface water depth (0.15 meters) in order to convert from areal units (i.e., g m^2 day^{-1}) to volumetric units (i.e., g m^3 day^{-1}):

$$GPP_{\text{daily}} \sim Normal(\mu = 20.7, \sigma = 40.0)$$

$$ER_{\text{daily}} \sim Normal(\mu = 47.3, \sigma = 47.3)$$

$$k_{600,\text{daily}} \sim Lognormal(\mu = 2.5, \sigma = 1.3)$$

$$\sigma_{obs} \sim HalfCauchy\,(\mu = 0, \sigma = 0.03, lower\ bound = 0, upper\ bound = \infty)$$

To sample the posterior distributions for the DO model, we used a NUTS sampler with a target acceptance statistic of 0.8. We used "cmdstanr", the R interface to Stan (Gabry et al., 2023), to run four MCMC chains each with 1,000 warmup samples and 1,000 saved samples.

Linear Models for Evaluating the Impacts of Caddisfly Density, GPP, and AER

We fit several linear models to assess the impact of caddisfly count on hyporheic exchange, overall net nitrate uptake, and streambed nitrate uptake, and the impacts of GPP and AER on overall net nitrate uptake. Because manipulation of mesocosm water volumes and flow-through characteristics on the day of the nitrate release would have led to erroneous estimates of GPP and AER on that day, we used estimates of GPP and AER from the day before the nitrate release, or September 16th, 2021 when evaluating the impact of GPP and AER on overall net nitrate uptake. Temperature and light were comparable on the day before and the day of the nitrate release, therefore we expect GPP and AER estimates from the day before the release to be representative of the relative differences in GPP and AER among mesocosms.

To estimate the intercept (β_0), slope (β_1), and residual error standard deviation (σ) parameters for each linear model, we used the brms package (Bürkner, 2017) as an R interface to Stan. We used the default priors from brms: an improper flat prior over the reals for β_1, a student's t distribution with a shape parameter of 3, a scale parameter of 2.5, and a location parameter equal to the median of the response variable for β_0, and a half student's t-distribution with a shape parameter of 3, a scale parameter of 2.5, a location parameter equal to 0, and a lower bound of 0 for σ. Since all response variables (i.e., hyporheic exchange rate, overall net nitrate uptake, and streambed nitrate uptake) were estimated by fitting models to the data as described above, we propagated the uncertainty in these estimates by specifying their standard

deviation in the "sdy" argument of the "mi" function from brms. Similarly, we propagated uncertainty in the predictors GPP and AER by specifying each estimate's standard deviation with the "sdx" argument of the "me" function from brms. We used a target acceptance rate of 0.9 and sampled each linear model using four MCMC chains each with 1,000 warmup samples and 2,000 saved samples.

Characterization of Bayesian Modeling Outputs

We verified MCMC chain convergence by visually inspecting trace plots and by calculating the $\hat{R}$ convergence diagnostic and bulk and tail effective sample size (ESS) using the rstan package (Stan Development Team, 2020). For each parameter estimate, we ensured that both bulk and tail ESS were at least 400 and that $\hat{R}$ was less than 1.01 (Vehtari et al., 2021). For all parameters estimated using Bayesian inference, we summarized the posterior by calculating the mean and 89% highest-density interval (HDI) across all MCMC samples. For all linear models, we also calculated Bayesian R-squared (Gelman et al., 2019) to provide an easy-to-interpret metric describing the estimated proportion of variance explained by each model. To interpret linear model parameter estimates and assess whether caddisflies had an effect on NO_x uptake, we used the framework outlined by (Makowski, Ben-Shachar, Chen, et al., 2019), which advocates for independently evaluating both whether an effect exists (referred to here as "effect existence"), and whether the effect is of a non-negligible magnitude (referred to here as "relative effect size").

We calculated the probability of direction ("pd") for each linear model's β_1 estimate as an index of effect existence. The pd is defined as the proportion of the posterior distribution that is either above zero if a majority of the posterior distribution is above zero, and below zero

otherwise (Makowski, Ben-Shachar, Chen, et al., 2019). Conceptually, it represents the probability that an effect is either positive or negative, whichever is more probable. We calculated the pd for each model using the "pd" function from the "bayestestR" package (Makowski, Ben-Shachar, & Lüdecke, 2019). As an index of relative effect size, we calculated percentage in the Region of Practice Equivalence ("ROPE") for each linear model's β_1 estimate. The percentage in the ROPE is defined as the percentage of the posterior distribution that overlaps with a range of values that are so close to zero that they lack practical relevance (Kruschke & Liddell, 2018; Makowski, Ben-Shachar, Chen, et al., 2019). To define the ROPE for each linear model's β_1, we first calculated the standard deviation of the response variable, divided by the standard deviation of the predictor, and multiplied by -0.1 and 0.1 to get the lower and upper bounds of the ROPE, respectively. Thus, the ROPE defines the region where a single standard deviation change in the predictor results in a predicted change in the response that is less than 10% of its standard deviation. We calculated the percentage in the ROPE for all linear models using the "ROPE" function from the "bayestestR" package (Makowski, Ben-Shachar, & Lüdecke, 2019). For brevity when reporting results, we refer the percentage in the ROPE as simply "ROPE".

RESULTS

Conservative Tracer Results

Background-Corrected SC

Following the addition of the tracer mass, SC rose almost instantaneously to between 93 and 151 μS cm^{-1} above background, equivalent to an added NaCl concentration of between 45 and 73 mg L^{-1}. During the next minute, SC displayed several distinct peaks (Figure 3a) indicating that the initially concentrated slug had completed another trip around the circular mesocosm channel. The peaks dampened over time as the solute dispersed. SC gradually reached a new steady-state by 20 minutes following the slug addition, indicating complete mixing between the streambed and surface water (Figure 3b).

To eliminate the effect of conservative tracer fluctuations during the first minute on inferences about hyporheic exchange, we fit equation (1) to the background-corrected salt concentration breakthrough curves measured between 1 and 20 minutes following the tracer release (Figure 3b). Differences in background-corrected salt concentrations at the steady-state beyond 20 minutes served as the basis for calculating mesocosm water volumes, which averaged 28.5 L and ranged from 24.4 to 35.9 L.

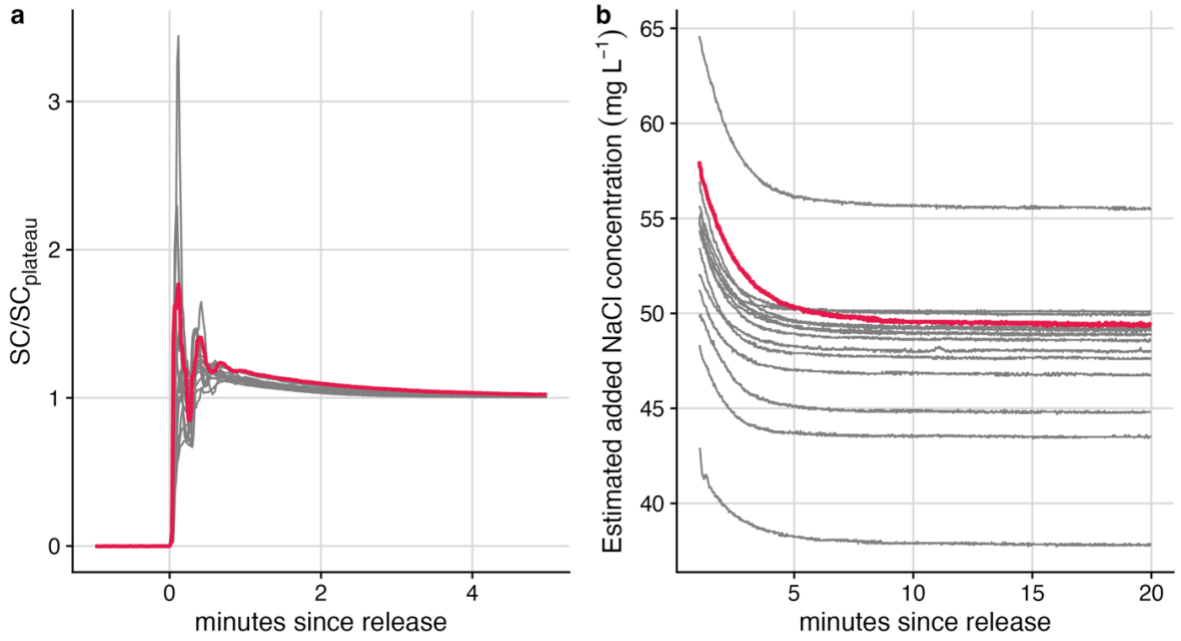

Figure 3. (a) SC measured just before and immediately following the NaCl release and normalized by the average SC measured between 30 and 60 minutes following the release. (b) Estimated background-corrected ("added") NaCl concentrations from between 1 and 20 minutes following the NaCl release. In both plots, each line represents data from a single mesocosm, with the red line highlighting the data from a representative mesocosm (0a) for demonstration purposes only.

Hyporheic Exchange Rates

SC posterior predictions reproduced patterns observed in the data (Appendix B Figure S1), with mean estimates of streambed surface-water exchange rate ranging from 3.0 L min^{-1} to 6.3 L min^{-1} (mean = 4.1 L min^{-1}). The effect of final caddisfly count on hyporheic exchange on the day of the nitrate release had a 96% chance of being positive, providing weak evidence for the existence of a caddisfly effect (Figure 4, Table 2). Further, the effect of caddisflies on hyporheic exchange could neither be considered negligible nor non-negligible (ROPE = 6.8%). Final caddisfly count explained 21% of the variance in hyporheic exchange rate.

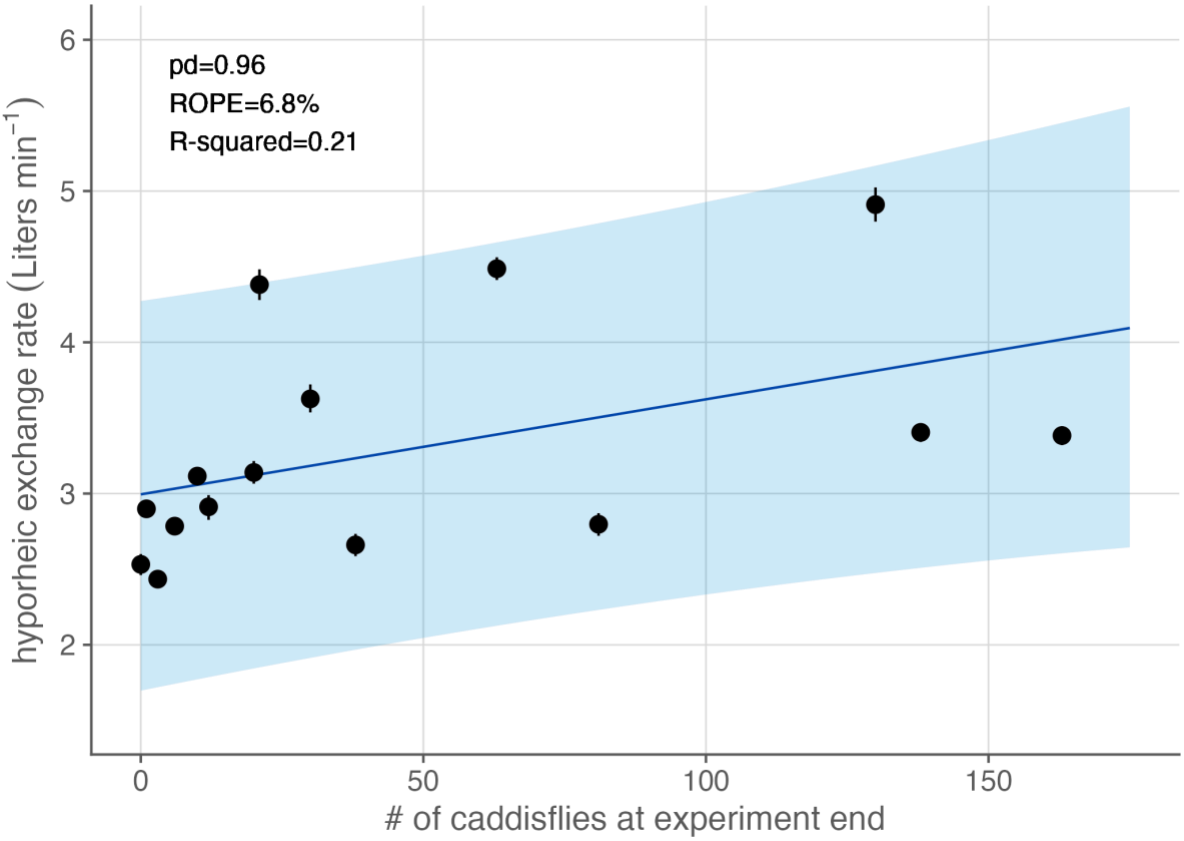

Figure 4. Mean estimated hyporheic exchange rate (points) and 89% highest-density credible intervals (vertical lines) for each mesocosm plotted against caddisfly counts. The blue line shows the mean predicted hyporheic exchange rate across all Markov Chain Monte Carlo samples and the blue area represents the 89% highest-density predictive interval.

Nitrate Results

Overall Net Nitrate Uptake

We observed low NO_x concentrations ranging from <1.5 to 7.5 ppb NO_x- N prior to the slug addition, which raised NO_x concentrations by 167.4 to 252.7 ppb NO_x- N (mean = 220.0 ppb NO_x- N). NO_x decreased steadily during the 24 hours following the nitrate release (Figure 5a). “Instantaneous” net nitrate uptake rates (i.e., the change in NO_x concentration divided by elapsed time) were variable within individual mesocosms and dropped strongly at concentrations

below ~50 ppb NO_x-N (Figure 5b). Mean estimates of overall net NO_x uptake rates ranged from 0.25 ppb NO_x- N/min to 0.74 ppb NO_x- N/min (mean = 0.43 ppb NO_x- N/min; Figure 6).

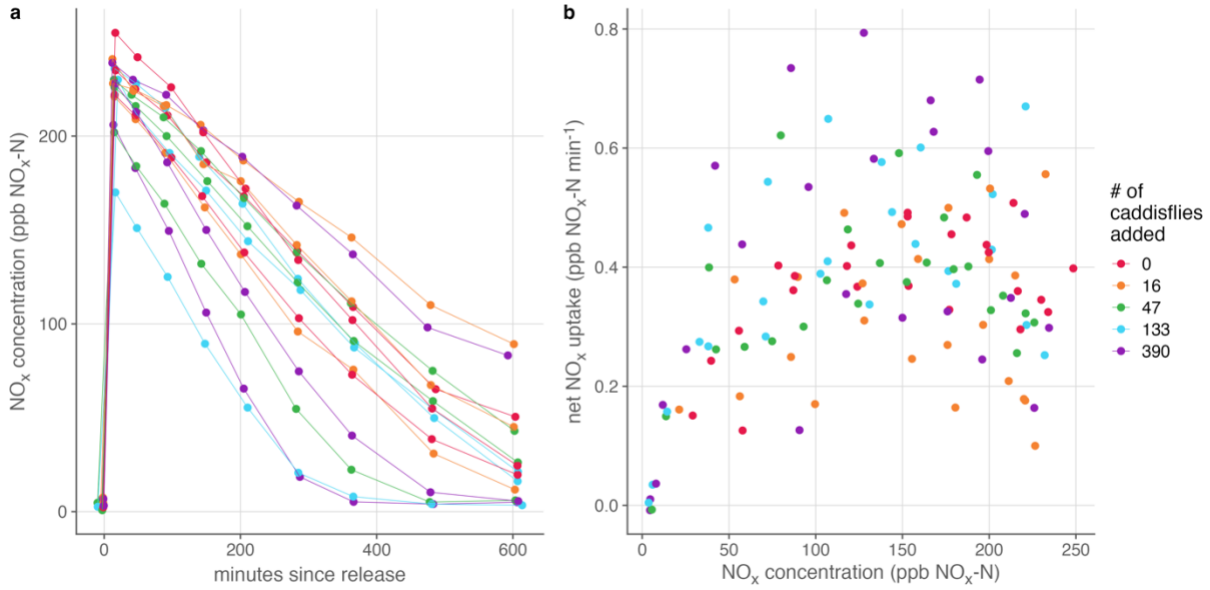

Figure 5. (a) Time series of NOx concentrations immediately before and following the nitrate release and (b) net NOx uptake rates (i.e., the change in NOx concentration divided by elapsed time) plotted against the average of NOx concentrations measured at the beginning and end of the elapsed time. At NOx concentrations < 50 ppb NOx-N, net NOx uptake rates diminished with decreasing concentration.

We found weak evidence for a positive effect (Figure 6, Table 2) of caddisflies on overall net nitrate uptake (pd = 0.96) suggesting that higher caddisfly densities are associated with higher rates of whole-mesocosm nitrate uptake, or faster nitrate removal (Figure 6). The effect of final caddisfly count on overall net nitrate uptake was of uncertain relative importance (ROPE = 6.2%), and final caddisfly count explained 23% of the variance in net nitrate uptake.

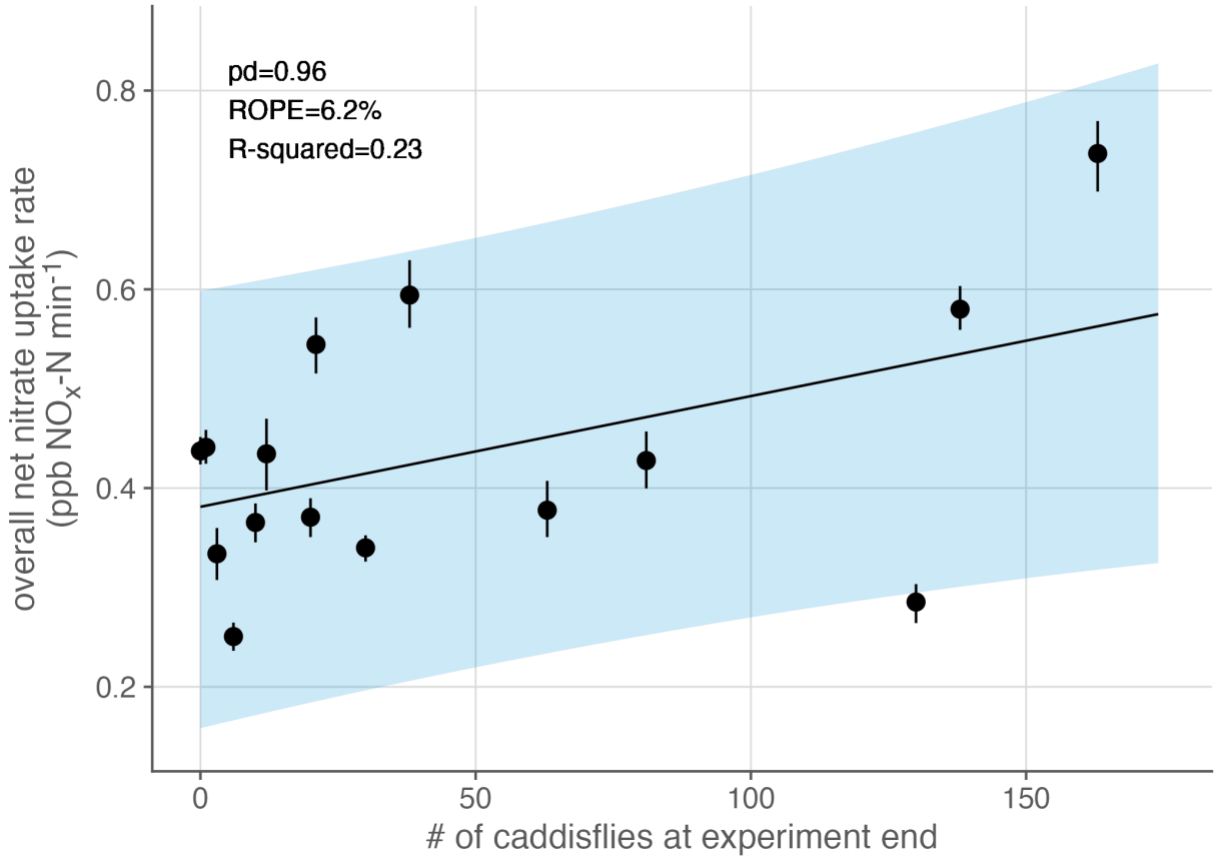

Figure 6. Estimated overall net nitrate uptake rates plotted against the number of caddisflies counted at the end of the experiment. Mean estimates are shown as points and 89% highest-density credible intervals are shown as vertical lines. The blue line shows the mean predicted nitrate uptake rate across all Markov Chain Monte Carlo samples and the blue area represents the 89% highest-density posterior predictive intervals.

Streambed Nitrate Uptake

NO_x concentration posterior predictions reproduced patterns in the data (Appendix B Figure S2), with mean estimates of streambed nitrate uptake rates ranging from 1.3 ppb NO_x-N/min to 3.7 ppb NO_x- N/min (mean = 2.2 ppb NO_x- N/min). The relationship between caddisflies and streambed net nitrate uptake (Figure 7; Table 2) was uncertain, with little evidence for an effect (pd = 0.84). Insufficient evidence (ROPE = 16.6%) was available to

suggest that the effect of caddisflies on streambed nitrate uptake was either negligible or non-negligible. Final caddisfly count explained 12% of the variance in streambed NOx uptake.

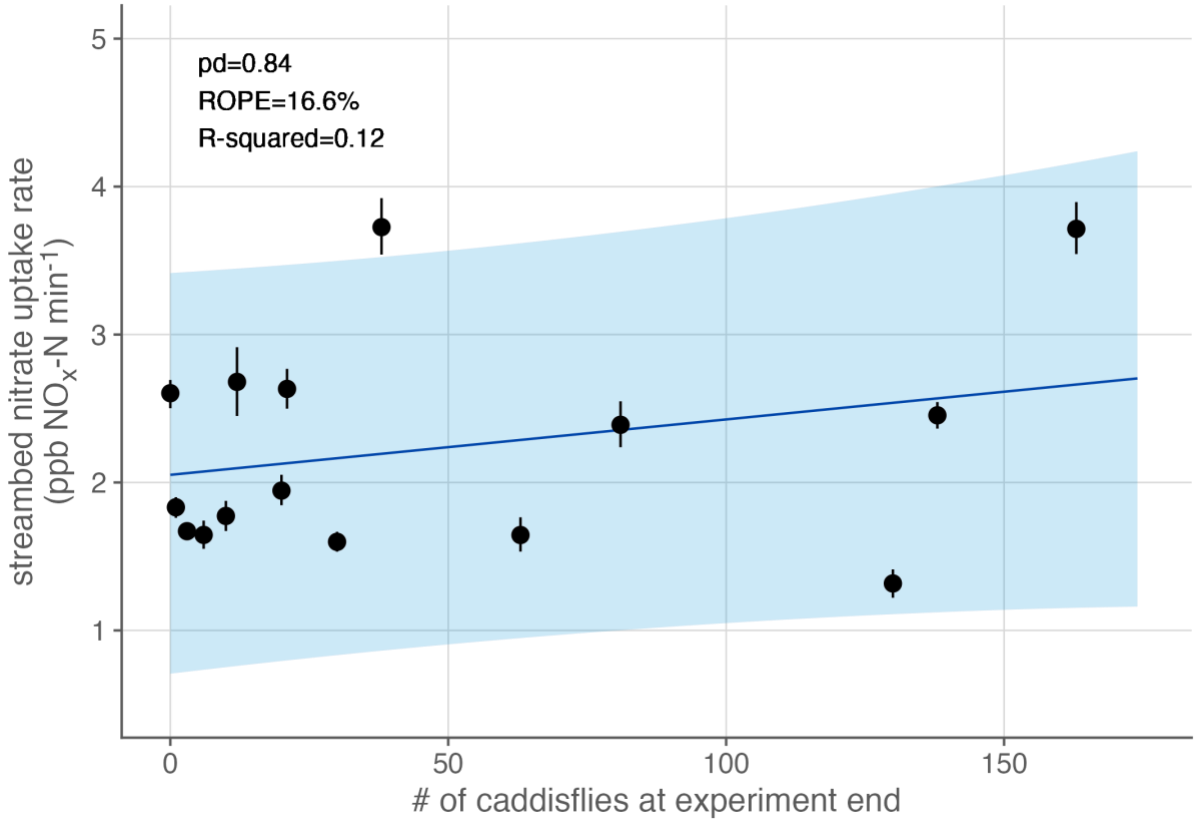

Figure 7. Estimated streambed nitrate uptake rates plotted against the number of caddisflies counted at the end of the experiment. Mean estimates are shown as points and 89% highest-density credible intervals are shown as vertical lines. The blue line shows mean predicted nitrate uptake rate across all Markov Chain Monte Carlo samples and the blue area represents the 89% highest-density posterior predictive interval.

Effect of GPP and AER on Nitrate Uptake

Metabolism models converged for each mesocosm on the day before the nitrate release, yielding posterior predictions that were reasonably consistent with measured DO concentrations (Figure S3). Mean estimates of AER ranged from -10.5 mg O_2 L^{-1} day^{-1} to -17.2 mg O_2 L^{-1} day^{-1} (mean = -13.1 mg O_2 L^{-1} day^{-1}), and mean estimates of GPP ranged from 5.8 mg O_2 L^{-1} day^{-1} to

8.7 mg O_2 L^{-1} day^{-1} (mean = 7.0 mg O_2 L^{-1} day^{-1}). While the effect of AER on overall net nitrate uptake was uncertain (pd = 0.91; Figure 8b), we observed a likely positive effect of GPP on overall net nitrate uptake (pd = 0.98; Figure 8a), implying that net NO_x removal occurred faster in mesocosms with higher rates of GPP. Both effects were of uncertain relative importance, with GPP having a stronger effect (ROPE = 4.0%) than AER (ROPE = 11.9%). Whereas AER explained 16% of the variance in overall net nitrate uptake, GPP explained 27%.

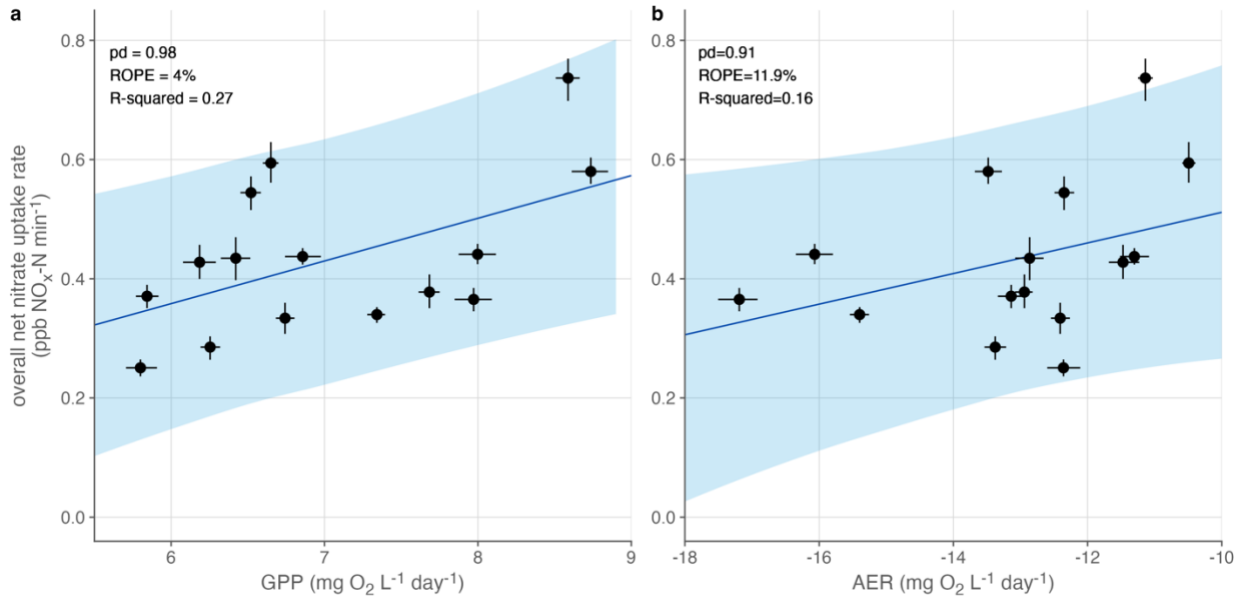

Figure 8. Estimated overall net nitrate uptake rates plotted against (a) estimated gross primary production and (b) aerobic ecosystem respiration on the day before the nitrate release. Mean estimates are shown as points and 89% highest-density credible intervals are shown as horizontal and vertical lines. Blue lines show the mean predicted nitrate uptake rate across all MCMC samples and blue areas represent 89% highest-density posterior predictive intervals.

Table 2. Summary statistics indicating effect existence and relative and absolute effect sizes for each model

Response	Predictor	pd	ROPE	R^2	Mean slope estimate	89% highest density credible interval
Hyporheic exchange ($L\ min^{-1}$)	Final # caddisflies	0.96	6.8%	0.21	6.3×10^{-3}	$[4.6 \times 10^{-4}, 1.2 \times 10^{-2}]$
Net NO_x uptake ($ppb\ NO_x\text{-}N\ min^{-1}$)	Final # caddisflies	0.96	6.2%	0.23	1.1×10^{-3}	$[9.1 \times 10^{-5}, 2.2 \times 10^{-3}]$
Streambed NO_x uptake ($ppb\ NO_x\text{-}N\ min^{-1}$)	Final # caddisflies	0.84	17.0%	0.12	3.7×10^{-3}	$[-2.3 \times 10^{-3}, 1.0 \times 10^{-2}]$
Net NO_x uptake ($ppb\ NO_x\text{-}N\ min^{-1}$)	Aerobic ecosystem respiration ($mg\ O_2\ L^{-1}\ day^{-1}$)	0.91	12.0%	0.16	7.2×10^{-2}	$[1.6 \times 10^{-2}, 1.3 \times 10^{-1}]$
Net NO_x uptake ($ppb\ NO_x\text{-}N\ min^{-1}$)	Gross primary production ($mg\ O_2\ L^{-1}\ day^{-1}$)	0.98	4.0%	0.27	2.6×10^{-2}	$[-5.0 \times 10^{-3}, 5.9 \times 10^{-2}]$

DISCUSSION

Relative Size of the Effect of Net-Spinning Caddisfly Larvae on Net Nitrate Uptake

Our experiments provided some evidence that higher densities of net-spinning caddisflies are associated with higher rates of overall net nitrate uptake. However, the relative importance of this effect was unclear. For the slope coefficient describing the effect of final caddisfly count on overall net nitrate uptake, the percent of the posterior distribution within the region or practical equivalence or "ROPE" was 6.2%, supporting neither the conclusion that the effect was negligible nor the conclusion that the effect was non-negligible (Makowski, Ben-Shachar, & Lüdecke, 2019).

However, we calculated the ROPE using the standard deviation of overall net nitrate uptake measured in our mesocosms. Thus, while the percentage in ROPE may be an appropriate measure of relative effect size in the context of our mesocosm experiments, it is inappropriate for assessing whether the potential effect of caddisflies on nitrate uptake would be appreciable in real stream ecosystems since it does not capture the full variability in nitrate uptake rates observed in natural streams and rivers. Moreover, we estimated nitrate uptake rates as a rate of concentration change, which varies with stream channel depth and often nitrate concentration. To compare the net nitrate uptake rate estimates from our mesocosms with those measured in real streams, we calculated nitrate uptake velocities using relationships from nutrient spiraling theory (Ensign & Doyle, 2006). Specifically, we calculated areal uptake flux by multiplying estimates of nitrate uptake rate – defined as rates of concentration change per time – by the mean estimated channel volume across all mesocosms (23 L) and then dividing by the surface area of the mesocosm stream channels (0.14 m^2). We then calculated uptake velocity as aerial uptake flux

divided by nitrate concentration. Here, it is reasonable to calculate uptake velocity for concentrations ranging from about 50 to 200 ppb NO_x-N since this is the range over which we observed relatively consistent NO_x uptake rates.

We estimated uptake velocities for the control (0 caddisflies m^{-2}) and for the highest caddisfly density treatment (2,500 caddisflies m^{-2}) using mean overall net nitrate uptake rates from the posterior predictive distribution (Figure 6). At a concentration of 100 ppb NO_x-N, estimated uptake velocities were 1.1 x 10^{-3} cm s^{-1} for the no-caddisfly case and 1.5 x 10^{-3} cm s^{-1} for the highest caddisfly density case. Both uptake velocities are comparable to those measured at similar concentrations across biomes in the LINX II study (Mulholland et al., 2008), illustrating that results from our mesocosm experiments may be comparable to natural streams. However, while total nitrate uptake velocities in the LINX II study spanned at least one order of magnitude at concentrations near 100 ppb NO_3^--N, estimated nitrate uptake velocities for the no-caddisfly and highest-density caddisfly cases spanned far less than an order of magnitude. This indicates that the impact of net-spinning caddisflies on total nitrate uptake is relatively small compared with variation in nitrate uptake across biomes and suggests that additional factors including primary production (Hall et al., 2009), streambed turbulence (Grant, Azizian, et al., 2018), and carbon availability (Arango et al., 2007; Bernhardt & Likens, 2002; L. T. Johnson et al., 2012) – among others – may be more important drivers of nitrate uptake than net-spinning caddisflies.

Sub-Optimal Conditions for Net-Spinning Caddisflies

While the effect of net-spinning caddisflies on overall net nitrate uptake may have been non-negligible, we found only weak evidence that the effect existed at all (pd = 0.96). If the

effect does exist and net-spinning caddisflies do enhance nitrate uptake, it is possible that effect sizes and evidence strength were weakened because conditions were suboptimal for the caddisflies, diminishing their ability to act as ecosystem engineers. This is consistent with relatively high levels of caddisfly mortality (Figure 2).

One possible explanation for caddisfly mortality and reduced engineering activity is that the net-spinning caddisflies in our experiments were experiencing heightened metabolic stress. Hydropsyche species common to the area where we collected those for our experiment, including *Hydropsyche cockarelli* and *Hydropsyche tana*, typically emerge and lay their eggs between late June and early August (Gustafson, 1990; Hauer & Stanford, 1982). Larvae progress through five instars (developmental stages), reaching terminal instar around October (Gustafson, 1990; Hauer & Stanford, 1982). We collected the caddisflies for our experiment at the beginning of September. Because the caddisflies were likely still growing and molting during this time, it may have been particularly difficult for them to acclimate to the mesocosms and to construct nets and retreats following removal from the sampled stream and introduction into the mesocosms.

However, previous mesocosm studies have also observed substantial net-spinning caddisfly larvae mortality, suggesting that additional factors beyond collection timing may have contributed to reduced engineering activity (Albertson et al., 2014, 2019; Fritz et al., 2023). For example, flow velocities in the mesocosm channels were likely non-ideal for caddisflies' net spinning activities. In two previous studies, individual *Hydropsyche* larvae were more likely to construct a net with increasing flow velocity for velocities ranging from 0.05 to 0.45 m/s (Loudon & Alstad, 1992; Philipson & Moorhouse, 1974). Specifically, Loudon and Alstad found that while just over 30% of the *Hydropsyche* larvae in their experiments spun nets at a flow

velocity of 0.05 m/s, about 90% of larvae spun nets at a velocity of 0.45 m/s. The same study also found that *Hydropsyche* larvae construct nets with a smaller mesh size (i.e., less coarse) at higher flow velocities (Loudon & Alstad, 1992). We estimated that the average channel flow velocities in our mesocosms were about 0.09 m/s, which is on the lower end of the experimental velocities used in the aforementioned studies. Thus, the relatively low flow velocities in our experiments may have led the caddisflies to spin fewer nets with coarser mesh size, reducing their potential impact on nitrate dynamics. Overall, our hypothesis about nitrate uptake was founded on the ecosystem engineering behavior of caddisflies and not the caddisflies themselves. Suboptimal experimental conditions may have limited caddisfly ecosystem engineering behavior, diminishing any potential effects on nitrate uptake.

Conceptualizing the Location of Nitrate Uptake in Streambeds

We did not find evidence that caddisflies had an effect on streambed nitrate uptake and thus we did not find support for our hypothesis that caddisflies affect nitrate uptake by altering streambed microbial activity. However, our estimates of streambed nitrate uptake were based on a set of modeling assumptions that may have been invalid. For example, our model (Equations 1 and 7) conceptualizes the mesocosm streambed and surface water channel as two separate domains that exchange water according to an exponential travel time distribution. We used this model along with conservative tracer data to estimate both streambed water volume and hyporheic exchange rate for each mesocosm rather than attempting to measure these quantities more directly. Hence, the streambed in the model is not necessarily confined to the physical region that we typically consider to be the streambed, but rather is defined as some arbitrary

volume of water that has exchanges with another well-mixed volume of water following an exponential travel time distribution.

The potential discrepancy between the model streambed extent and the physical streambed extent is particularly consequential since our model also assumes that all nitrate uptake occurs in the streambed. For instance, if mesocosm surface water mixed rapidly with the shallow benthos – e.g., via turbulence (Grant, Gomez-Velez, et al., 2018) – the model would have characterized the shallow benthos as surface water, thus underestimating the physical streambed extent. In this case, nitrate uptake would be attributed to an artificially small volume and the streambed nitrate uptake rate would be overestimated. Additionally, the magnitude of overestimation likely varied among mesocosms due to random differences in the physical characteristics of each mesocosm.

Yet even if the model accurately represents the extent of the streambed, we have several reasons to believe that much of the nitrate uptake occurred at the streambed-surface water interface and shallow benthos rather than occurring homogeneously within the streambed. First, we found moderate evidence that higher GPP was associated with higher nitrate uptake rates (Figure 8; Table 2). This suggests that at least some of the nitrate uptake was driven by assimilation by autotrophs living at the streambed-surface water interface, consistent with findings from streams across multiple biomes (Hall et al., 2009). Second, dissolved oxygen concentrations remained relatively high throughout the course of the experiment; DO levels measured in the surface water were at 94% of saturation on average and never dropped below 80% saturation. Moreover, we estimated that the mean streambed travel time across mesocosms was 1.8 minutes, with 94% of the water across all mesocosms exchanging at timescales of 5

minutes or less. The combination of dissolved oxygen levels near saturation and relatively short streambed travel times likely diminished the importance of streambed denitrification, since denitrification primarily occurs in anoxic zones that likely become more prevalent in subsurface flowpaths with longer travel times (Zarnetske et al., 2011).

Finally, previous research conducted in real streams has demonstrated that a substantial proportion of nitrate uptake occurs at the streambed-surface water interface and in shallow sediments (Battin, Kaplan, Newbold, & Hendricks, 2003; Harvey et al., 2013; Knapp et al., 2017). Such findings highlight inhomogeneity in nitrate uptake within the streambed and may partially explain why many researchers have been unable to empirically demonstrate a relationship between transient storage and nutrient uptake (Hall et al., 2002; Lautz & Siegel, 2007; Ward & Packman, 2019). While others have attributed this lack of empirical relationship to other less metabolically-active forms of surface transient storage like dead zones and side pools (Ensign & Doyle, 2006; Hall et al., 2002), our circular mesocosms were effectively channelized and had very little visible surface transient storage. Thus, this research adds to the body of evidence suggesting the need for more robust ways to represent and scale nitrate uptake occurring in diverse hydrologic domains including the surface water-streambed interface and shallow subsurface (Covino, 2017; Harvey et al., 2013; Ward & Packman, 2019).

If nitrate uptake in our mesocosms was in fact occurring primarily at the streambed-surface water interface rather than deeper in the subsurface, then the number of caddisflies inhabiting the streambed surface should serve as a more representative indicator of the potential for caddisflies to affect overall net nitrate uptake rate. We conducted a preliminary analysis relating overall net nitrate uptake rate with sampled surface-dwelling caddisflies (Appendix D

Figure S7). Results from this analysis were inconclusive and warrant further analysis that accounts for sampling error in surface-dwelling caddisfly counts.

Sensitivity of Nitrate Uptake to Hyporheic Exchange Rate

Previous research has shown that *Hydropsyche* larvae and their silk structures can measurably reduce the hydraulic conductivity of sediment relative to controls (MacDonald et al., 2020). This finding suggests that, in addition to the mechanism discussed in this paper, caddisflies could also influence nitrate uptake rates by altering the rate and timescale of hyporheic exchange. However, because our mesocosms had a fixed volume, mean streambed travel time and exchange rate were inversely related (i.e., $Q = \frac{V}{\overline{\tau}}$). While an increase in streambed travel time would theoretically allow longer time for reactions to proceed in the biologically active streambed, an increase in mean travel time also corresponds to a reduction in hyporheic exchange rate, which controls the rate of delivery of biologically active solutes to the streambed. Thus, for reactions whose rates are constant with respect to hyporheic travel time, the effect of increased travel time on nitrate uptake would be counteracted by the effect of a corresponding decrease in hyporheic exchange rate.

This point can be further illustrated by considering the reaction significance factor (RSF), a metric that quantifies the relative contribution of a single hydrologic domain to whole-stream biogeochemistry (Gomez-Velez et al., 2015; Harvey et al., 2013; Harvey & Fuller, 1998). The RSF is conventionally defined as $RSF = Da\frac{L}{L_s} = \overline{\tau}\, k_1 \frac{L}{L_s} = \frac{\overline{\tau}}{\tau_{reac}}\frac{L}{L_s}$, where Da is the Damköhler number of the hydrologic domain of interest, $\overline{\tau}$ is mean travel time, k_1 is the first-order reaction rate constant, τ_{reac} is the characteristic reaction timescale, L is a reference length,

and L_s is turnover length, or the average distance a solute molecule travels before exchanging with the hydrologic domain of interest. Considering our mesocosm streambeds as the hydrologic domain of interest, an increase in the rate constant k within the streambed would yield a higher RSF. Conversely, an increase in mean streambed travel time may not yield a higher RSF if it occurs in conjunction with an increase in turnover length, which is expected for our mesocosms since they have a fixed subsurface water volume. Thus, the RSF model suggests that our experimental setup and modeling methods were potentially suitable for assessing whether caddisflies affected overall nitrate uptake by influencing streambed microbial activity, since whole mesocosm nitrate uptake would be sensitive to changes in streambed uptake rate. In contrast, our experimental methods may be less appropriate for assessing whether caddisflies impact nitrate uptake by reducing rates of hyporheic exchange, since overall nitrate uptake would not be sensitive to changes in hyporheic exchange rate.

Recommendations

We recommend that future work using a similar study design consider the following recommendations for improvement upon this study. First, we recommend creating more favorable conditions for the net-spinning caddisflies by maintaining flow velocities of at least 0.2 m/s and by collecting the caddisfly larvae after they have reached terminal instar (between October and July in our sample stream). Second, when modeling the mesocosms, we recommend constraining streambed water volume using physical measurements such as sediment porosity and volume, which could be incorporated into the model as informative priors. In order to obtain reasonable model fits with these additional constraints, it may be necessary to represent

hyporheic travel time distributions differently, such as using a non-parametric model (Payn et al., 2008).

Third, rather than assuming that all nitrate uptake occurs in the streambed homogeneously, future research should represent heterogeneity in nitrate uptake rates throughout the entire mesocosm. Future models might include separate terms for nitrate uptake in the streambed and nitrate uptake in surface water and at the streambed-surface water interface (Briggs et al., 2009; Z. C. Johnson et al., 2015). However, disentangling these two terms would likely require additional data collection and could add potential model over-parameterization. One approach would be to maintain flow through each mesocosm, allow nitrate concentrations to reach steady state, and collect water samples from multiple depths in the mesocosm streambed. This would allow for estimation of streambed uptake rates (O'Connor & Harvey, 2008), which could then be compared with overall net nitrate uptake rates measured using e.g., $^{15}N\text{-}NO_3$ tracer addition and surface water sampling (Mulholland et al., 2004). Another approach would be to characterize the relationship between hyporheic travel time and nitrate uptake rate, which could also be facilitated via collection of subsurface water samples (Harvey et al., 2013; Zarnetske et al., 2011). Using this approach, one could adapt the model used for this study (Equation 7) to consider differences in nitrate uptake rate as a function of hyporheic travel time. This would make it possible to scale the effect of mesocosm streambed nitrate uptake to model how streambed uptake contributes to overall net nitrate uptake.

Finally, we recommend that future research consider modifying the experimental setup to create more anaerobic zones and thus greater potential for denitrification. This could be achieved by modifying sediment size distributions, increasing ambient nutrient concentration, or

adding organic matter to the sediment (Inwood et al., 2007; Mulholland et al., 2008; Solomon et al., 2009). The reaction significance factor (RSF) described above assumes that reactions can be described with some rate constant that does not vary with respect to travel time for the hydrologic domain of interest. While this assumption may be reasonable for assimilatory nitrate uptake, it may be a poor assumption for denitrification, which tends to occur only after oxygen has been consumed and therefore may not begin until some threshold travel time (Zarnetske et al., 2011). If this were the case, increased mean hyporheic travel time could result in increased whole-mesocosm denitrification despite associated reductions in hyporheic exchange rate. This suggests that if denitrification represented a larger fraction of nitrate uptake in the mesocosms, it would be possible to examine how caddisflies mediate nitrate uptake by altering hydrologic exchange.

CONCLUSION

In this study, we hypothesized that net-spinning caddisfly larvae enhance whole-stream nitrate uptake by increasing the capacity of the streambed microbial community to take up nitrate. We tested this hypothesis by experimentally manipulating caddisfly density in a set of stream-analogue mesocosms, conducting nitrate releases in each mesocosm, and using models and Bayesian inference to estimate whole-mesocosm and streambed nitrate uptake rates. Experimental results provided weak evidence that higher caddisfly densities were associated with higher rates of whole-mesocosm nitrate uptake but provided little evidence that caddisflies increased streambed nitrate uptake rates. We found moderate evidence that gross primary production (GPP) was positively associated with whole-mesocosm nitrate uptake rates, indicating that much of the nitrate uptake in our mesocosms was occurring at the photosynthetically active streambed surface-water interface. Overall, our study demonstrates modest potential for net-spinning caddisfly larvae to act as ecosystem engineers by altering nitrate uptake rates in experimental mesocosms. Future work could use a modified experimental setup and modeling approach to lend additional evidence to our findings.

REFERENCES CITED

Albertson, L. K., Cardinale, B. J., & Sklar, L. S. (2014). Non-Additive Increases in Sediment Stability Are Generated by Macroinvertebrate Species Interactions in Laboratory Streams. *PLoS ONE*, *9*(8), e103417. https://doi.org/10.1371/journal.pone.0103417

Albertson, L. K., Sklar, L. S., Cooper, S. D., & Cardinale, B. J. (2019). Aquatic macroinvertebrates stabilize gravel bed sediment: A test using silk net-spinning caddisflies in semi-natural river channels. *PLoS ONE*, *14*(1), e0209087. https://doi.org/10.1371/journal.pone.0209087

Appling, A. P., Hall, R. O., Yackulic, C. B., & Arroita, M. (2018). Overcoming Equifinality: Leveraging Long Time Series for Stream Metabolism Estimation. *Journal of Geophysical Research: Biogeosciences*, *123*(2), 624–645. https://doi.org/10.1002/2017jg004140

Appling, A. P., Read, J. S., Winslow, L. A., Arroita, M., Bernhardt, E. S., Griffiths, N. A., et al. (2018). The metabolic regimes of 356 rivers in the United States. *Scientific Data*, *5*(1), 180292. https://doi.org/10.1038/sdata.2018.292

Arango, C. P., Tank, J. L., Schaller, J. L., Royer, T. V., Bernot, M. J., & David, M. B. (2007). Benthic organic carbon influences denitrification in streams with high nitrate concentration. *Freshwater Biology*, *52*(7), 1210–1222. https://doi.org/10.1111/j.1365-2427.2007.01758.x

Bastviken, D., Persson, L., Odham, G., & Tranvik, L. (2004). Degradation of dissolved organic matter in oxic and anoxic lake water. *Limnology and Oceanography*, *49*(1), 109–116. https://doi.org/10.4319/lo.2004.49.1.0109

Basu, N. B., Meter, K. J. V., Byrnes, D. K., Capellen, P. V., Brouwer, R., Jacobsen, B. H., et al. (2022). Managing nitrogen legacies to accelerate water quality improvement. *Nature Geoscience*, *15*(2), 97–105. https://doi.org/10.1038/s41561-021-00889-9

Battin, T. J., Kaplan, L. A., Newbold, J. D., & Hendricks, S. P. (2003). A mixing model analysis of stream solute dynamics and the contribution of a hyporheic zone to ecosystem function*. *Freshwater Biology*, *48*(6), 995–1014. https://doi.org/10.1046/j.1365-2427.2003.01062.x

Battin, T. J., Kaplan, L. A., Newbold, J. D., & Hansen, C. M. E. (2003). Contributions of microbial biofilms to ecosystem processes in stream mesocosms. *Nature*, *426*(6965), 439–442. https://doi.org/10.1038/nature02152

Bernhardt, E. S., & Likens, G. E. (2002). Dissolved organic carbon enrichment alters nitrogen dynamics in a forest stream. *Ecology*, *83*(6), 1689–1700. https://doi.org/10.1890/0012-9658(2002)083[1689:docean]2.0.co;2

Bertagnolli, A. D., Maritan, A. J., Tumolo, B. B., Fritz, S. F., Oakland, H. C., Mohr, E. J., et al. (2023). Net-spinning caddisflies create denitrifier-enriched niches in the stream microbiome. ISME Communications, 3(1), 111. https://doi.org/10.1038/s43705-023-00315-8

Boulton, A. J., Datry, T., Kasahara, T., Mutz, M., & Stanford, J. A. (2010). Ecology and management of the hyporheic zone: stream-groundwater interactions of running waters and their floodplains. *Journal of the North American Benthological Society*, *29*(1), 26–40. https://doi.org/10.1899/08-017.1

Breemen, N. van, Boyer, E. W., Goodale, C. L., Jaworski, N. A., Paustian, K., Seitzinger, S. P., et al. (2002). Where did all the nitrogen go? Fate of nitrogen inputs to large watersheds in the northeastern U.S.A. *Biogeochemistry*, *57–58*(1), 267–293. https://doi.org/10.1023/a:1015775225913

Briggs, M. A., Gooseff, M. N., Arp, C. D., & Baker, M. A. (2009). A method for estimating surface transient storage parameters for streams with concurrent hyporheic storage. *Water Resources Research*, *45*(4). https://doi.org/10.1029/2008wr006959

Briggs, M. A., Day-Lewis, F. D., Zarnetske, J. P., & Harvey, J. W. (2015). A physical explanation for the development of redox microzones in hyporheic flow. *Geophysical Research Letters*, *42*(11), 4402–4410. https://doi.org/10.1002/2015gl064200

Burgin, A. J., & Hamilton, S. K. (2007). Have we overemphasized the role of denitrification in aquatic ecosystems? A review of nitrate removal pathways. Frontiers in Ecology and the Environment, 5(2), 89–96. https://doi.org/10.1890/1540-9295(2007)5[89:HWOTRO]2.0.CO;2

Bürkner, P.-C. (2017). brms : An R Package for Bayesian Multilevel Models Using Stan. *Journal of Statistical Software*, *80*(1). https://doi.org/10.18637/jss.v080.i01

Cardinale, B. J., Gelmann, E. R., & Palmer, M. A. (2004). Net spinning caddisflies as stream ecosystem engineers: the influence of Hydropsyche on benthic substrate stability. *Functional Ecology*, *18*(3), 381–387. https://doi.org/10.1111/j.0269-8463.2004.00865.x

Carpenter, B., Gelman, A., Hoffman, M. D., Lee, D., Goodrich, B., Betancourt, M., et al. (2017). Stan : A Probabilistic Programming Language. *Journal of Statistical Software*, *76*(1). https://doi.org/10.18637/jss.v076.i01

Covino, T. (2017). Hydrologic connectivity as a framework for understanding biogeochemical flux through watersheds and along fluvial networks. *Geomorphology*, *277*, 133–144. https://doi.org/10.1016/j.geomorph.2016.09.030

Diaz, R. J., & Rosenberg, R. (2008). Spreading Dead Zones and Consequences for Marine Ecosystems. *Science*, *321*(5891), 926–929. https://doi.org/10.1126/science.1156401

Dodds, W. K., Bouska, W. W., Eitzmann, J. L., Pilger, T. J., Pitts, K. L., Riley, A. J., et al. (2009). Eutrophication of U.S. Freshwaters: Analysis of Potential Economic Damages. *Environmental Science & Technology*, *43*(1), 19-Dec. https://doi.org/10.1021/es801217q

Ensign, S. H., & Doyle, M. W. (2006). Nutrient spiraling in streams and river networks. *Journal of Geophysical Research: Biogeosciences (2005–2012)*, *111*(G4). https://doi.org/10.1029/2005jg000114

Fritz, S. F., Albertson, L. K., Hobgood, J. L., Mohr, E. J., Oakland, H. C., & Poole, G. C. (2023). Macroinvertebrate ecosystem engineering affects streambed retention of microplastics. *Freshwater Science*, *42*(2), 133–145. https://doi.org/10.1086/724584

Gabry, J., Češnovar, R., & Johnson, A. (2023). cmdstanr: R Interface to "CmdStan." Retrieved from https://mc-stan.org/cmdstanr/

Garcia, H. E., & Gordon, L. I. (1992). Oxygen solubility in seawater: Better fitting equations. *Limnology and Oceanography*, *37*(6), 1307–1312. https://doi.org/10.4319/lo.1992.37.6.1307

Ge, H., Xu, K., & Ghahramani, Z. (2018). Turing: a language for flexible probabilistic inference. In *International Conference on Artificial Intelligence and Statistics, AISTATS 2018, 9-11 April 2018, Playa Blanca, Lanzarote, Canary Islands, Spain* (pp. 1682–1690). Retrieved from http://proceedings.mlr.press/v84/ge18b.html

Gelman, A., Goodrich, B., Gabry, J., & Vehtari, A. (2019). R-squared for Bayesian Regression Models. *The American Statistician*, *73*(3), 307–309. https://doi.org/10.1080/00031305.2018.1549100

Gomez-Velez, J. D., Harvey, J. W., Cardenas, M. B., & Kiel, B. (2015). Denitrification in the Mississippi River network controlled by flow through river bedforms. *Nature Geoscience*, *8*(12), 941–945. https://doi.org/10.1038/ngeo2567

Gonzalez-Pinzon, R., Dorley, J., Horn, D. V., Garayburu-Carusso, V., & Stegen, J. (2021). *Physical, resource supply, and biological controls on nutrient processing along the river continuum*. United States. Retrieved from https://www.osti.gov/biblio/1860260

Grant, S. B., Azizian, M., Cook, P., Boano, F., & Rippy, M. A. (2018). Factoring stream turbulence into global assessments of nitrogen pollution. *Science*, *359*(6381), 1266–1269. https://doi.org/10.1126/science.aap8074

Grant, S. B., Gomez-Velez, J. D., & Ghisalberti, M. (2018). Modeling the Effects of Turbulence on Hyporheic Exchange and Local-to-Global Nutrient Processing in Streams. *Water Resources Research*, *54*(9), 5883–5889. https://doi.org/10.1029/2018wr023078

Guo, C., Liu, X., & He, X. (2022). A global meta-analysis of crop yield and agricultural greenhouse gas emissions under nitrogen fertilizer application. *Science of The Total Environment*, *831*, 154982. https://doi.org/10.1016/j.scitotenv.2022.154982

Gustafson, D. L. (1990). Ecology of Aquatic Insects in the Gallatin River Drainage. Montana State University. Retrieved from https://scholarworks.montana.edu/xmlui/handle/1/7184

Hall, R. O. Jr., Peterson, B. J., & Meyer, J. L. (1998). Testing a Nitrogen-Cycling Model of a Forest Stream by Using a Nitrogen-15 Tracer Addition. *Ecosystems*, *1*(3), 283–298. https://doi.org/10.1007/s100219900022

Hall, R. O. Jr., Bernhardt, E. S., & Likens, G. E. (2002). Relating nutrient uptake with transient storage in forested mountain streams. *Limnology and Oceanography*, *47*(1), 255–265. https://doi.org/10.4319/lo.2002.47.1.0255

Hall, R. O. Jr., Tank, J. L., Sobota, D. J., Mulholland, P. J., O'Brien, J. M., Dodds, W. K., et al. (2009). Nitrate removal in stream ecosystems measured by 15N addition experiments: Total uptake. *Limnology and Oceanography*, *54*(3), 653–665. https://doi.org/10.4319/lo.2009.54.3.0653

Hall, R. O. Jr., Tank, J. L., Baker, M. A., Rosi-Marshall, E. J., & Hotchkiss, E. R. (2016). Metabolism, Gas Exchange, and Carbon Spiraling in Rivers. *Ecosystems*, *19*(1), 73–86. https://doi.org/10.1007/s10021-015-9918-1

Hallegraeff, G. (2003). Harmful algal blooms: a global overview. *Manual on Harmful Marine Microalgae*, *33*, 22-Jan.

Harvey, J. W., & Fuller, C. C. (1998). Effect of enhanced manganese oxidation in the hyporheic zone on basin-scale geochemical mass balance. *Water Resources Research*, *34*(4), 623–636. https://doi.org/10.1029/97wr03606

Harvey, J. W., Böhlke, J. K., Voytek, M. A., Scott, D., & Tobias, C. R. (2013). Hyporheic zone denitrification: Controls on effective reaction depth and contribution to whole-stream mass balance. *Water Resources Research*, *49*(10), 6298–6316. https://doi.org/10.1002/wrcr.20492

Hastings, A., Byers, J. E., Crooks, J. A., Cuddington, K., Jones, C. G., Lambrinos, J. G., et al. (2007). Ecosystem engineering in space and time. *Ecology Letters*, *10*(2), 153–164. https://doi.org/10.1111/j.1461-0248.2006.00997.x

Hauer, F. R., & Stanford, J. A. (1982). Ecology and Life Histories of Three Net-Spinning Caddisfly Species (Hydropsychidae:Hydropsyche) in the Flathead River, Montana. *Freshwater Invertebrate Biology*, *1*(4), 18–29. https://doi.org/10.2307/1467138

Hauer, F. R., Locke, H., Dreitz, V. J., Hebblewhite, M., Lowe, W. H., Muhlfeld, C. C., et al. (2016). Gravel-bed river floodplains are the ecological nexus of glaciated mountain landscapes. *Science Advances*, *2*(6), e1600026. https://doi.org/10.1126/sciadv.1600026

Helton, A. M., Ardón, M., & Bernhardt, E. S. (2015). Thermodynamic constraints on the utility of ecological stoichiometry for explaining global biogeochemical patterns. *Ecology Letters*, *18*(10), 1049–1056. https://doi.org/10.1111/ele.12487

Hemphill, N. (1988). Competition between two stream dwelling filter-feeders, Hydropsyche oslari and Simulium virgatum. *Oecologia*, *77*(1), 73–80. https://doi.org/10.1007/bf00380928

Hinkle, S. R., Duff, J. H., Triska, F. J., Laenen, A., Gates, E. B., Bencala, K. E., et al. (2001). Linking hyporheic flow and nitrogen cycling near the Willamette River — a large river in Oregon, USA. *Journal of Hydrology*, *244*(3–4), 157–180. https://doi.org/10.1016/s0022-1694(01)00335-3

Inwood, S. E., Tank, J. L., & Bernot, M. J. (2007). Factors Controlling Sediment Denitrification in Midwestern Streams of Varying Land Use. *Microbial Ecology*, *53*(2), 247–258. https://doi.org/10.1007/s00248-006-9104-2

Jähne, B., Münnich, K. O., Bösinger, R., Dutzi, A., Huber, W., & Libner, P. (1987). On the parameters influencing air-water gas exchange. *Journal of Geophysical Research: Oceans*, *92*(C2), 1937–1949. https://doi.org/10.1029/jc092ic02p01937

Johnson, L. T., Royer, T. V., Edgerton, J. M., & Leff, L. G. (2012). Manipulation of the Dissolved Organic Carbon Pool in an Agricultural Stream: Responses in Microbial Community Structure, Denitrification, and Assimilatory Nitrogen Uptake. *Ecosystems*, *15*(6), 1027–1038. https://doi.org/10.1007/s10021-012-9563-x

Johnson, Z. C., Warwick, J. J., & Schumer, R. (2015). Nitrogen retention in the main channel and two transient storage zones during nutrient addition experiments. *Limnology and Oceanography*, *60*(1), 57–77. https://doi.org/10.1002/lno.10006

Jones, C. G., Lawton, J. H., & Shachak, M. (1994). Organisms as Ecosystem Engineers. *Oikos*, *69*(3), 373. https://doi.org/10.2307/3545850

Juras, M., Albertson, L. K., Cahoon, J., & Johnson, E. (2018). Incorporating macroinvertebrate biological structures into gravel-bedded stream fluid dynamics using 3D CFD modelling. *Ecological Engineering*, *119*, 19–28. https://doi.org/10.1016/j.ecoleng.2018.05.011

Knapp, J. L. A., González-Pinzón, R., Drummond, J. D., Larsen, L. G., Cirpka, O. A., & Harvey, J. W. (2017). Tracer-based characterization of hyporheic exchange and benthic biolayers in streams. *Water Resources Research*, *53*(2), 1575–1594. https://doi.org/10.1002/2016wr019393

Kruschke, J. K., & Liddell, T. M. (2018). The Bayesian New Statistics: Hypothesis testing, estimation, meta-analysis, and power analysis from a Bayesian perspective. *Psychonomic Bulletin & Review*, *25*(1), 178–206. https://doi.org/10.3758/s13423-016-1221-4

Lautz, L. K., & Siegel, D. I. (2007). The effect of transient storage on nitrate uptake lengths in streams: an inter-site comparison. *Hydrological Processes*, *21*(26), 3533–3548. https://doi.org/10.1002/hyp.6569

Li, A., Bernal, S., Kohler, B., Thomas, S. A., Martí, E., & Packman, A. I. (2021). Residence Time in Hyporheic Bioactive Layers Explains Nitrate Uptake in Streams. *Water Resources Research*, *57*(2). https://doi.org/10.1029/2020wr027646

Loudon, C., & Alstad, D. N. (1992). Architectural plasticity in net construction by individual caddisfly larvae (Trichoptera: Hydropsychidae). *Canadian Journal of Zoology*, *70*(6), 1166–1172. https://doi.org/10.1139/z92-163

MacDonald, M. J., Albertson, L. K., & Poole, G. C. (2020). Ecosystem engineering in the streambed: Net-spinning caddisflies influence hydraulic properties. *Ecohydrology*. https://doi.org/10.1002/eco.2266

Makowski, D., Ben-Shachar, M., & Lüdecke, D. (2019). bayestestR: Describing Effects and their Uncertainty, Existence and Significance within the Bayesian Framework. *Journal of Open Source Software*, *4*(40), 1541. https://doi.org/10.21105/joss.01541

Makowski, D., Ben-Shachar, M. S., Chen, S. H. A., & Lüdecke, D. (2019). Indices of Effect Existence and Significance in the Bayesian Framework. *Frontiers in Psychology*, *10*, 2767. https://doi.org/10.3389/fpsyg.2019.02767

Morse, J. C., Frandsen, P. B., Graf, W., & Thomas, J. A. (2019). Diversity and Ecosystem Services of Trichoptera. *Insects*, *10*(5), 125. https://doi.org/10.3390/insects10050125

Mulholland, P. J., Valett, H. M., Webster, J. R., Thomas, S. A., Cooper, L. W., Hamilton, S. K., & Peterson, B. J. (2004). Stream denitrification and total nitrate uptake rates measured using a field 15N tracer addition approach. *Limnology and Oceanography*, *49*(3), 809–820. https://doi.org/10.4319/lo.2004.49.3.0809

Mulholland, P. J., Helton, A. M., Poole, G. C., Hall, R. O., Hamilton, S. K., Peterson, B. J., et al. (2008). Stream denitrification across biomes and its response to anthropogenic nitrate loading. *Nature*, *452*(7184), 202–205. https://doi.org/10.1038/nature06686

O'Connor, B. L., & Harvey, J. W. (2008). Scaling hyporheic exchange and its influence on biogeochemical reactions in aquatic ecosystems. *Water Resources Research*, *44*(12). https://doi.org/10.1029/2008wr007160

Opperman, J. J., Orr, S., Baleta, H., Dailey, M., Garrick, D., Goichot, M., et al. (2018). *Valuing Rivers:How the diverse benefits of healthy rivers underpin economies*. WWF.

Payn, R. A., Gooseff, M. N., Benson, D. A., Cirpka, O. A., Zarnetske, J. P., Bowden, W. B., et al. (2008). Comparison of instantaneous and constant-rate stream tracer experiments through non-parametric analysis of residence time distributions. *Water Resources Research*, *44*(6). https://doi.org/10.1029/2007wr006274

Philipson, G. N., & Moorhouse, B. H. S. (1974). Observations on ventilatory and net-spinning activities of larvae of the genus Hydropsyche Pictet (Trichoptera, Hydropsychidae) under experimental conditions. *Freshwater Biology*, *4*(6), 525–533. https://doi.org/10.1111/j.1365-2427.1974.tb00112.x

Rackauckas, C., & Nie, Q. (2016). DifferentialEquations.jl – A Performant and Feature-Rich Ecosystem for Solving Differential Equations in Julia. *Journal of Open Research Software*, *5*(1), 15. https://doi.org/10.5334/jors.151

Raymond, P. A., Zappa, C. J., Butman, D., Bott, T. L., Potter, J., Mulholland, P., et al. (2012). Scaling the gas transfer velocity and hydraulic geometry in streams and small rivers. *Limnology and Oceanography: Fluids and Environments*, *2*(1), 41–53. https://doi.org/10.1215/21573689-1597669

Schlesinger, W. H., Reckhow, K. H., & Bernhardt, E. S. (2006). Global change: The nitrogen cycle and rivers: NITROGEN CYCLE AND RIVERS. *Water Resources Research*, *42*(3). https://doi.org/10.1029/2005wr004300

Seitzinger, S., Harrison, J. A., Böhlke, J. K., Bouwman, A. F., Lowrance, R., Peterson, B., et al. (2006). Denitrification across landscapes and waterscapes: a synthesis. *Ecological Applications*, *16*(6), 2064–2090. https://doi.org/10.1890/1051-0761(2006)016[2064:dalawa]2.0.co;2

Smith, V. H. (2003). Eutrophication of freshwater and coastal marine ecosystems a global problem. *Environmental Science and Pollution Research*, *10*(2), 126–139. https://doi.org/10.1065/espr2002.12.142

Solomon, C. T., Hotchkiss, E. R., Moslemi, J. M., Ulseth, A. J., Stanley, E. H., Hall, R. O., & Flecker, A. S. (2009). Sediment size and nutrients regulate denitrification in a tropical stream. *Journal of the North American Benthological Society*, *28*(2), 480–490. https://doi.org/10.1899/07-157.1

Stan Development Team. (2020). RStan: the R interface to Stan. Retrieved from http://mc-stan.org/

Tumolo, B. B., Albertson, L. K., Cross, W. F., Poole, G. C., Davenport, G., Daniels, M. D., & Sklar, L. S. (2023). Resource modification by ecosystem engineers generates hotspots of stream community assembly and ecosystem function. *Ecology*, *104*(6), e4052. https://doi.org/10.1002/ecy.4052

Vehtari, A., Gelman, A., Simpson, D., Carpenter, B., & Bürkner, P.-C. (2021). Rank-Normalization, Folding, and Localization: An Improved $\hat{R}$ for Assessing Convergence of MCMC. *Bayesian Analysis*, *16*(2). https://doi.org/10.1214/20-ba1221

Vitousek, P. M., Aber, J. D., Howarth, R. W., Likens, G. E., Matson, P. A., Schindler, D. W., et al. (1997). Human alteration of the global nitrogen cycle: sources and consequences. Ecological Applications, 7(3), 737–750. https://doi.org/10.2307/2269431

Ward, A. S., & Packman, A. I. (2019). Advancing our predictive understanding of river corridor exchange. *Wiley Interdisciplinary Reviews: Water*, *6*(1). https://doi.org/10.1002/wat2.1327

Wurtsbaugh, W. A., Paerl, H. W., & Dodds, W. K. (2019). Nutrients, eutrophication and harmful algal blooms along the freshwater to marine continuum. *Wiley Interdisciplinary Reviews: Water*, *6*(5). https://doi.org/10.1002/wat2.1373

Zarnetske, J. P., Haggerty, R., Wondzell, S. M., & Baker, M. A. (2011). Dynamics of nitrate production and removal as a function of residence time in the hyporheic zone. *Journal of Geophysical Research: Biogeosciences (2005–2012)*, *116*(G1). https://doi.org/10.1029/2010jg001356

Zarnetske, J. P., Haggerty, R., Wondzell, S. M., Bokil, V. A., & González-Pinzón, R. (2012). Coupled transport and reaction kinetics control the nitrate source-sink function of hyporheic zones. *Water Resources Research*, *48*(11). https://doi.org/10.1029/2012wr011894

Zhang, X., Ward, B. B., & Sigman, D. M. (2020). Global Nitrogen Cycle: Critical Enzymes, Organisms, and Processes for Nitrogen Budgets and Dynamics. *Chemical Reviews*, *120*(12), 5308–5351. https://doi.org/10.1021/acs.chemrev.9b00613

APPENDICES

APPENDIX A

ANALYTICAL SOLUTION TO CONSERVATIVE TRACER MODEL

Here, I derive the analytical solution of the following ordinary differential equation using Laplace transforms:

$$\frac{dC}{dt} = q\left(\int_0^t g(\tau)C(t\ -\ \tau)\ d\tau\ - C(t)\right) + C_0\delta(t - t_{add})$$

The streambed travel time distribution is defined as:

$$g(\tau) =\ \lambda e^{-\lambda t}$$

Switching to a more standard notation (i.e., C(t) = f(t)) and substituting in g(τ), we obtain:

$$f'(t) = q\left(\int_0^t \lambda e^{-\lambda t} f(t\ -\ \tau)\ d\tau\ - f(t)\right) + C_0\delta(t - t_{add})$$

The Laplace transform of this is:

$$sF(s) - f(0) = q\big(F(s)G(s) - F(s)\big) + C_{add}e^{-t_{add}s}$$

The Laplace transform of the streambed travel time distribution is:

$$G(s) = \frac{\lambda}{s +\ \lambda}$$

We define t_{add} as 0 such that t = 0 at the moment the conservative tracer is added. Considering this definition and substituting in G(s) we get:

$$sF(s) - qF(s)\frac{\lambda}{s+\lambda} + qF(s) = C_{add} + f(0)$$

We can then rearrange and simplify:

$$F(s)(s - q\frac{\lambda}{s+\lambda} + q) = C_{add} + f(0)$$

$$F(s) = \frac{C_{add} + f(0)}{\left(s - \frac{q\lambda}{s+\lambda} + q\right)} = \frac{(C_{add} + f(0))(s+\lambda)}{s^2 +\ \lambda s - q\lambda + qs + q\lambda} = \frac{(C_{add} + f(0))(s+\lambda)}{s^2 + s(\lambda + q)}$$

Completing the square and formatting the numerator so it has an inverse Laplace transform yields the following:

$$F(s) = \frac{(C_{add} + f(0))(s+\lambda)}{\left(s+\frac{\lambda+q}{2}\right)^2 - \left(\frac{\lambda+q}{2}\right)^2} = \frac{(C_{add} + f(0))(s+\frac{\lambda+q}{2} + \lambda - \frac{\lambda+q}{2})}{\left(s-\frac{-(\lambda+q)}{2}\right)^2 - \left(\frac{\lambda+q}{2}\right)^2}$$

The above can be simplified by defining and substituting two additional variables (a and b):

$$a = -\frac{\lambda+q}{2} \qquad b = \frac{\lambda+q}{2}$$

$$F(s) = (C_{add} + f(0))\left[\frac{(s-a)}{(s-a)^2 - b^2} + \frac{\lambda-q}{\lambda+q}\frac{b}{(s-a)^2 - b^2}\right]$$

We can take the inverse Laplace transform to get:

$$f(t) = (C_{add} + f(0))\left[e^{at}\cosh(bt) + \frac{\lambda-q}{\lambda+q}e^{at}\sinh(bt)\right]$$

Plugging a and b back in and simplifying yields the analytical solution the Equation 1:

$$f(t) = (C_{add} + f(0))e^{-\frac{(\lambda+q)t}{2}}\left[\cosh\left(\frac{\lambda+q}{2}t\right) + \frac{\lambda-q}{\lambda+q}\sinh\left(\frac{\lambda+q}{2}t\right)\right]$$

APPENDIX B

POSTERIOR PREDICTIONS

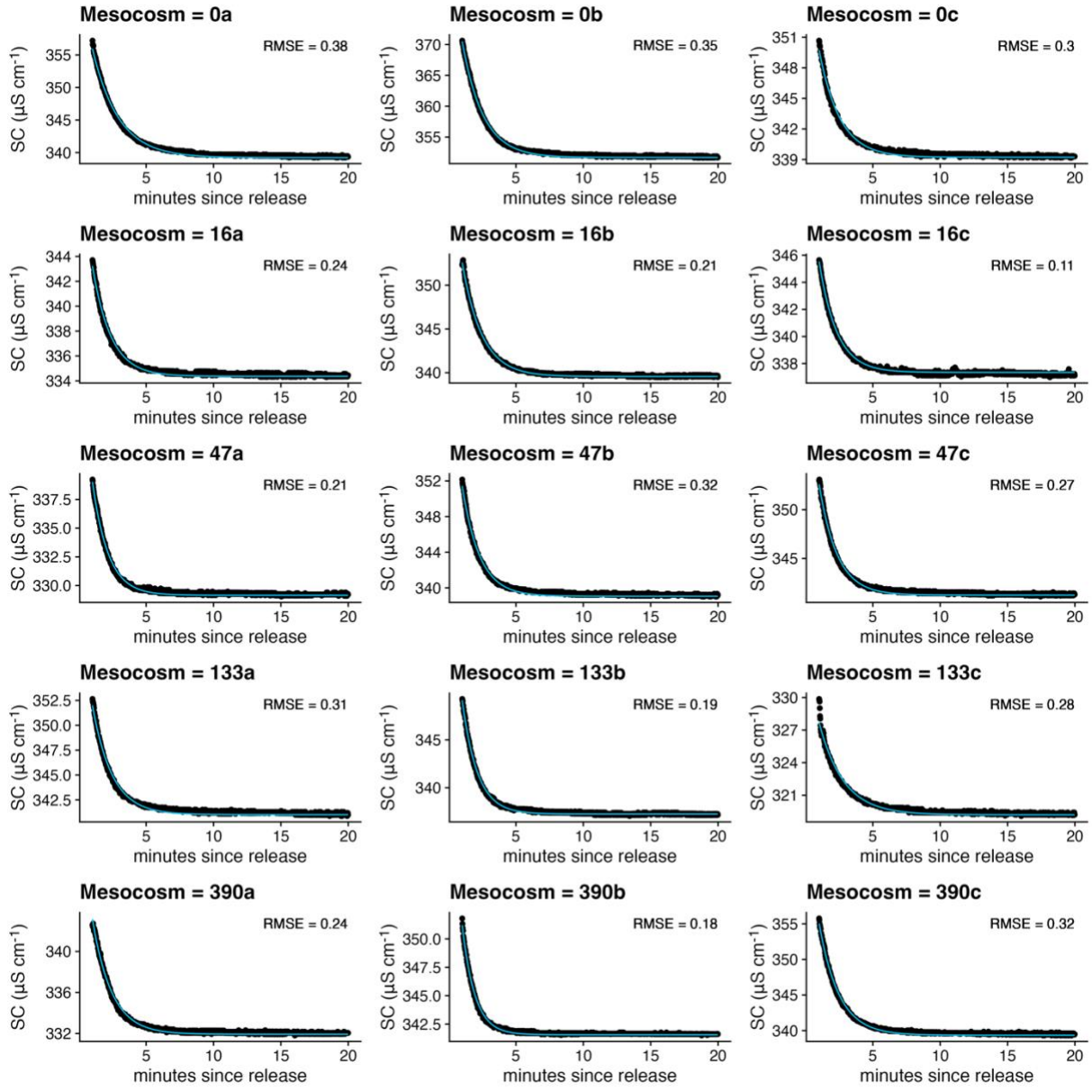

Figure S1. Observed SC (black points), mean posterior prediction (turquoise line), and 89% highest-density posterior predictive intervals (grey areas). For SC, posterior predictive intervals are sufficiently small and difficult if not impossible to see. To calculate RMSE for each MCMC sample, we first modeled SC without process or measurement error by running the process-based model (i.e., Equation 1) using each sample's parameter set and saving the model output at all times when SC was measured. We then quantified the difference between measured and modeled SC by calculating root mean squared error (RMSE) for each MCMC sample. The RMSE value shown on each plot represents the median RMSE across all MCMC samples.

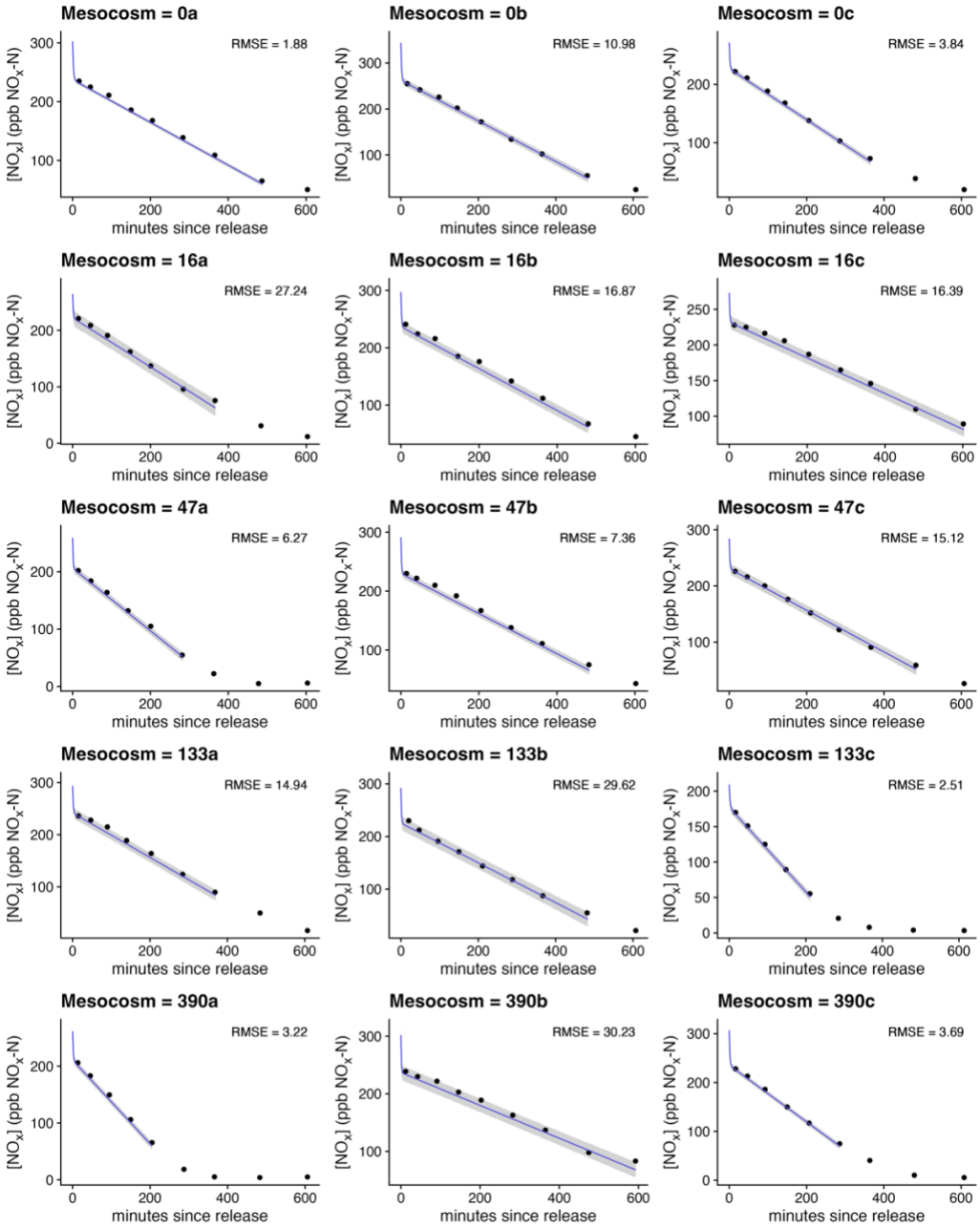

Figure S2. Observed NOx concentrations (black points), mean posterior prediction (indigo line), and 89% highest-density posterior predictive intervals (grey areas). To calculate RMSE for each MCMC sample, we first modeled NOx without process or measurement error by running the process-based model (i.e., Equation 7) using each sample's parameter set and saving the model output at all times when NOx was measured. We then quantified the difference between measured and modeled NOx by calculating root mean squared error (RMSE) for each MCMC sample. The RMSE value shown on each plot represents the median RMSE across all MCMC samples.

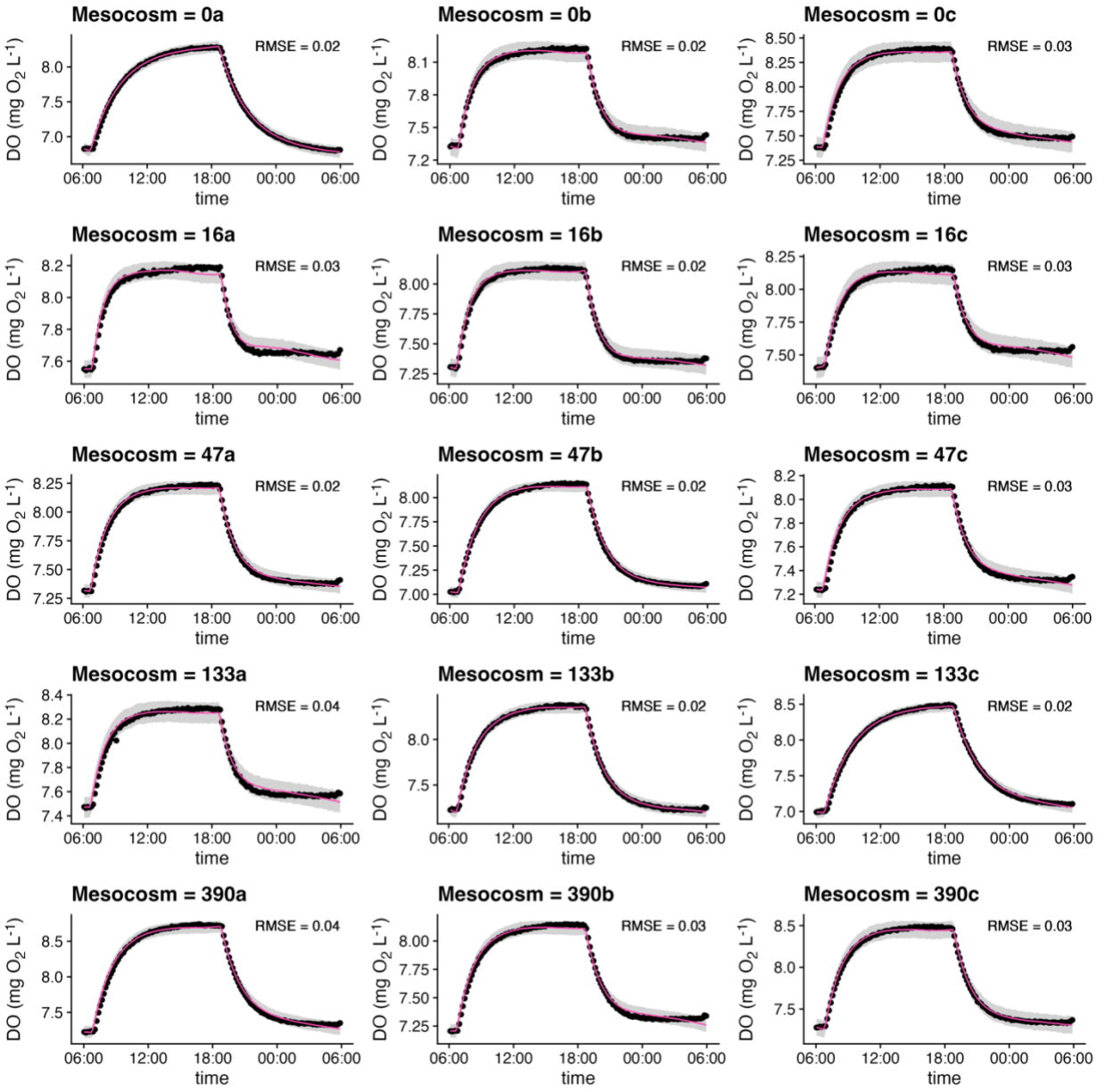

Figure S3. Observed DO concentrations (black points), mean posterior prediction (pink line), and 89% highest-density posterior predictive intervals (grey areas) for September 16, 2021. For each MCMC sample, we modeled DO concentration by running the process-based model (i.e., Equation 8) using that sample's parameter set and saving the model output at all times when DO was measured. We then quantified the difference between measured and modeled DO by calculating root mean squared error (RMSE) for each MCMC sample. The RMSE value shown on each plot represents the median RMSE across all MCMC samples.

APPENDIX C

RESULTS SHOWN WITH CADDISFLY TREATMENT AS A PREDICTOR

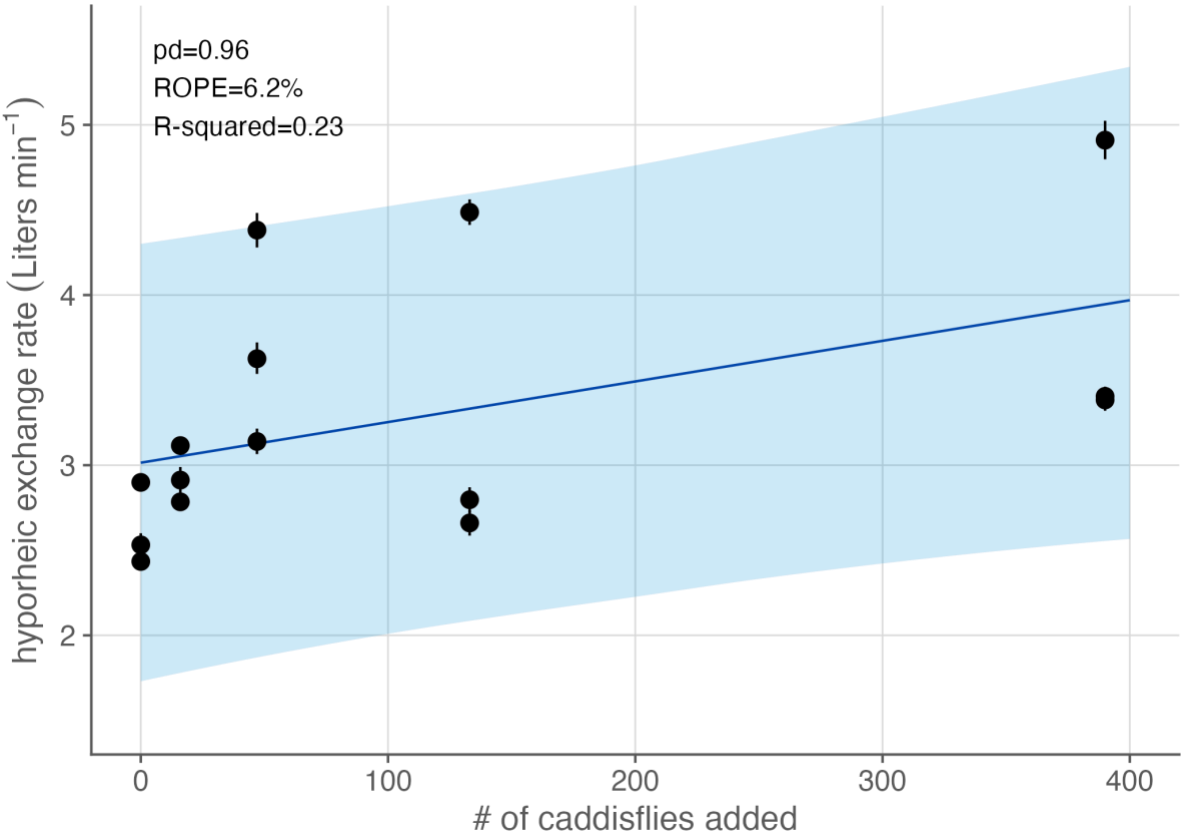

Figure S4. Estimated hyporheic exchange rate plotted against caddisfly treatment. Mean estimates are shown as points and 89% highest-density credible intervals are shown as vertical lines. The blue line shows mean predicted hyporheic exchange rate across all Markov Chain Monte Carlo samples and the blue area represents the 89% highest-density posterior predictive interval.

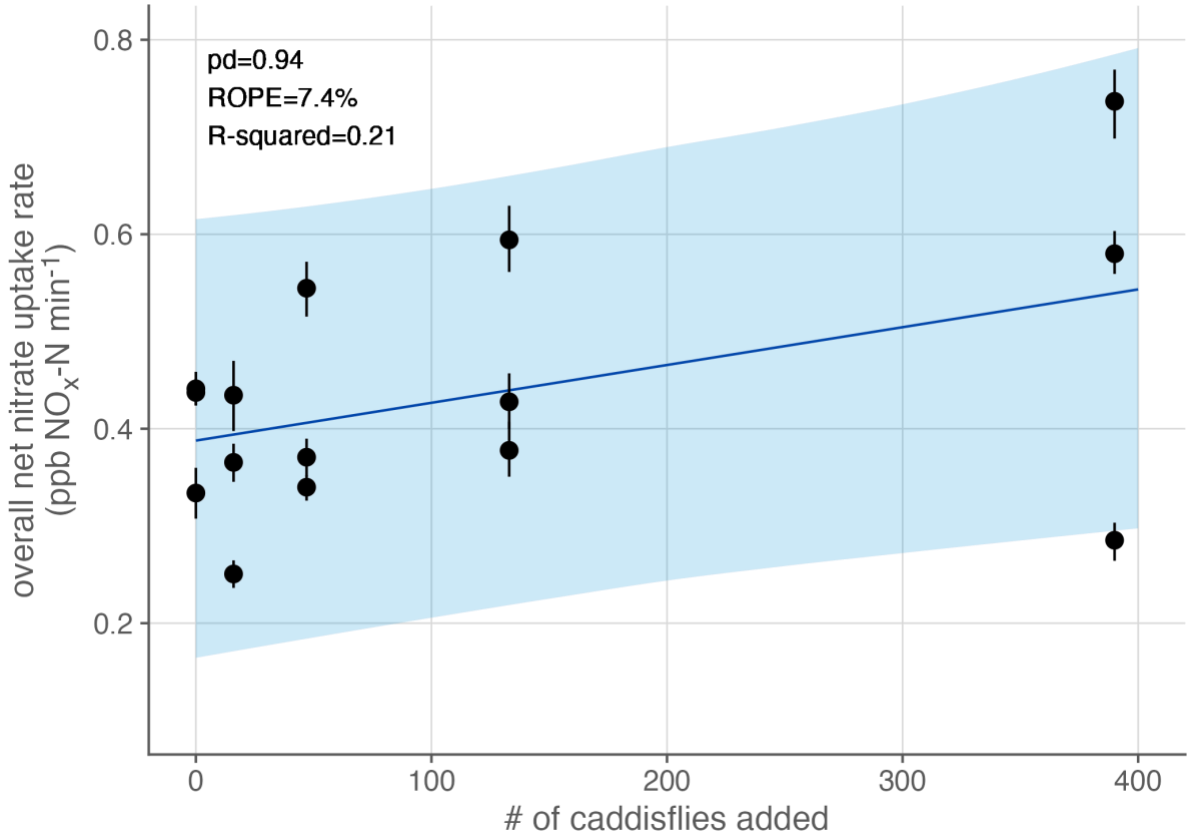

Figure S5. Estimated overall net nitrate uptake rate plotted against caddisfly treatment. Mean estimates are shown as points and 89% highest-density credible intervals are shown as vertical lines. The blue line shows mean predicted overall net nitrate uptake rate across all Markov Chain Monte Carlo samples and the blue area represents the 89% highest-density posterior predictive interval.

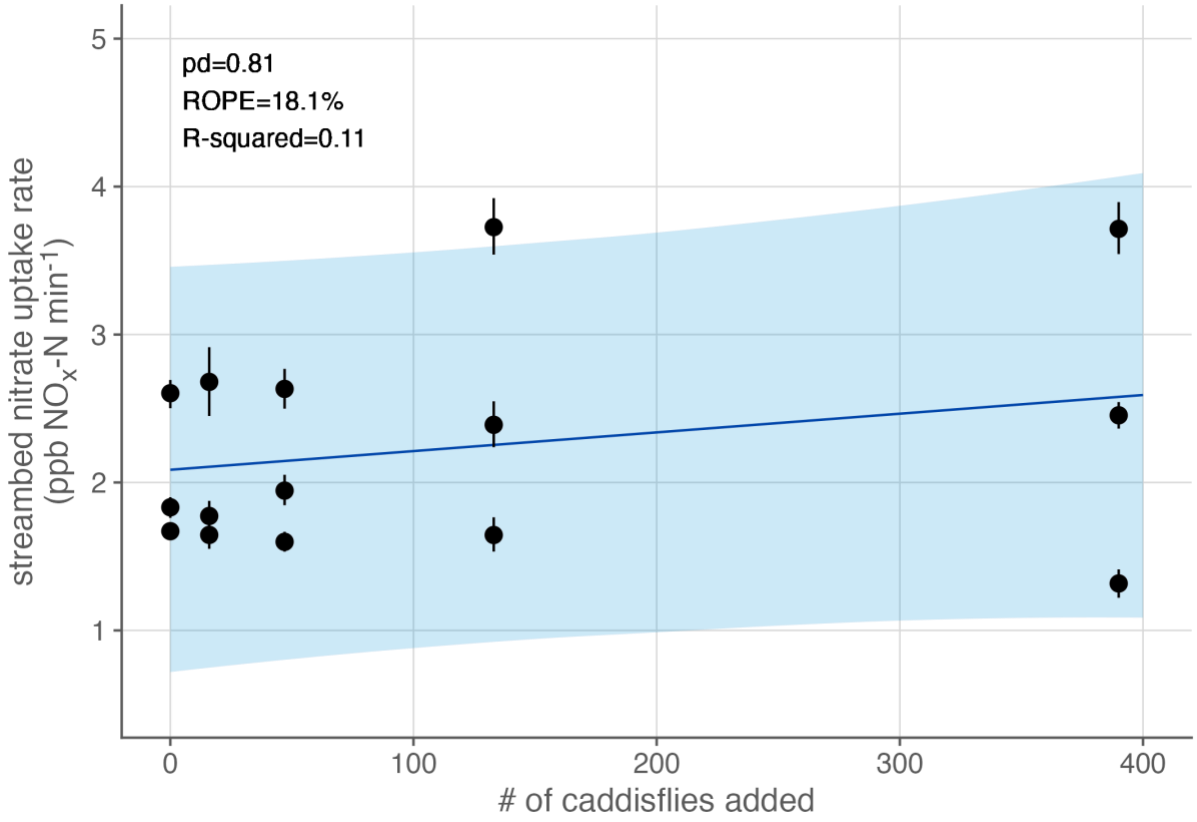

Figure S6. Estimated streambed nitrate uptake rate plotted against caddisfly treatment. Mean estimates are shown as points and 89% highest-density credible intervals are shown as vertical lines. The blue line shows mean predicted streambed nitrate uptake rate across all Markov Chain Monte Carlo samples and the blue area represents the 89% highest-density posterior predictive interval.

APPENDIX D

NITRATE UPTAKE VS SAMPLED SURFACE CADDISFLY COUNTS

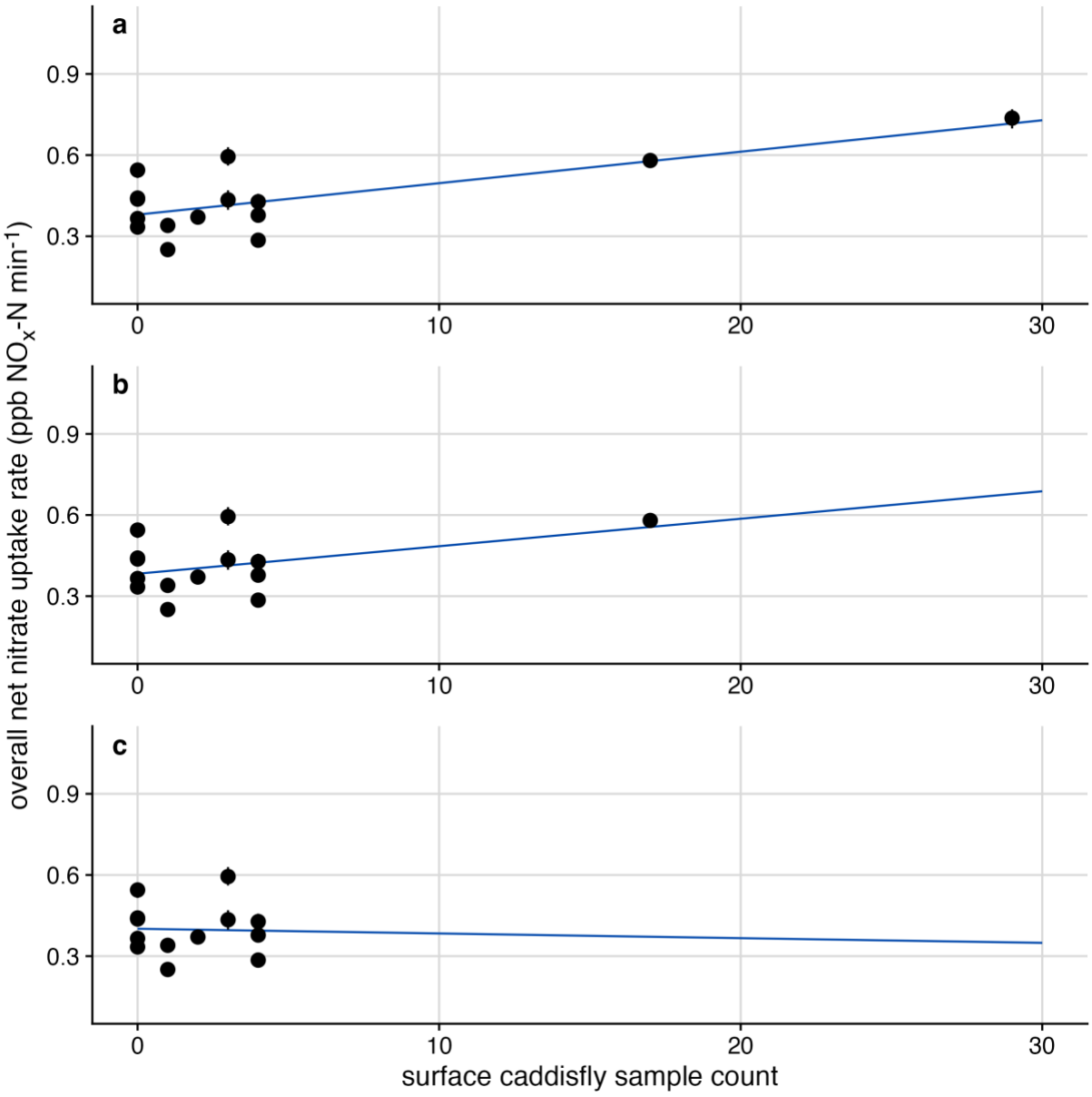

Figure S7. Estimated overall net nitrate uptake rate plotted against caddisflies sampled from the top layer of rocks on the mesocosm surface. Mean uptake estimates for each mesocosm are shown as points and 89% highest-density credible intervals are shown as vertical lines. The surface caddisfly count on the x-axis does not represent the total number of caddisflies present on the surface of the streambed, but rather represents the total number of caddisflies counted from four samples collected from a total area of approximately 435 cm2, or about 30% of the total mesocosm streambed area. Blue lines represent linear regression fits with (a) data from all mesocosms, (b) the highest sample count removed, and (c) the highest two sample counts removed.